



# Geochemistry of magnetite in beach sands, stream sediments, and in situ magnetites in surrounding rocks at north Taiwan island

Eslam Mohammed Ali Mitwally<sup>1,2</sup> · Bing-Sheng Yu<sup>1</sup>

Received: 30 August 2021 / Revised: 24 November 2021 / Accepted: 5 December 2021 / Published online: 6 January 2022  
© The Author(s), under exclusive licence to Science Press and Institute of Geochemistry, CAS and Springer-Verlag GmbH Germany, part of Springer Nature 2022

**Abstract** The geochemistry of magnetite provides constraints on the source(s) of the magnetite and other ore minerals. In this study, we constructed a magnetite distribution map, compared the chemical composition of magnetite present in hard rocks with that present in sand beach and stream deposits to determine magnetite's provenance, investigated relationships among different trace elements, examined variations in the concentrations of trace elements present in magnetite, and identified the type of studied magnetite. Laser ablation inductively coupled plasma mass spectrometry (LA-ICP-MS) and inductively coupled plasma mass spectrometry/inductively coupled plasma atomic emission spectroscopy was used to analyze samples available in small and large amounts, respectively. The average magnetite compositions of beach and river samples were substantially similar to those of andesite rocks, revealing that the magnetite samples may have originated from surrounding andesite rocks; this finding is consistent with the chemical composition of the samples analyzed using LA-ICP-MS. Some of the andesite rocks found in the study area were the primary source of magnetite aggregations in the beach sands and stream sands near or slightly away from these rocks. High Ti–V magnetites lie within the fields of Fe–Ti–V bearing magnetite and titanomagnetite (ulvöspinel). These titanomagnetites may be undergoing transformation to spinel minerals such as galaxite,

gahnite, magnesiochromite, and chromite, which are characterized by the high concentrations of Al, Ti, Mg, Cr, Ni, Mn, and Zn. The positive correlation between Fe and Ti, Cr and Ni, and also the negative correlation between Fe and Mg, Mn and Zn can be attributed to various magnetite phases present in the study area. V, Co, Mo, Nb, Ga, Sn, and Ta exhibited a positive correlation with Fe and a negative correlation with Al. The positive correlation between Fe and these elements indicates the enrichment of these elements in the magnetite series. We observed a negative correlation between Fe and Li, Rb, Ca, Ba, Sr, Cu, Cd, Sb, As, Sc, Y, REE, U, and Th. A positive correlation between Al and these elements indicates the enrichment of these elements in the spinel series.

**Keywords** Magnetite chemistry · LA-ICP-MS · Element incorporation · Multi variation diagram · Distribution map · North Taiwan

## 1 Introduction

The chemistry of magnetite will be affected during weathering, diagenesis, and metamorphism processes (Abdullah and Atherton 1964; Luepke 1980; Morton and Hallsworth 1994; Maier and Barnes 1996). The magnetite crystallographic structure is stable under low temperature and pressure (Morton 1991). By contrast, the magnetite structure is less stable (Buddington and Lindsley 1964) during high-grade metamorphism, and magnetite can gain some elements such as Ti, V, Cr, and Zn (Sun et al. 2019). Therefore, alterations in the magnetite structure are related to the degree of metamorphism and the original composition of the host rock. A low Ti concentration in magnetite

✉ Eslam Mohammed Ali Mitwally  
t107799401@ntut.org.tw

<sup>1</sup> Institute of Mineral Resources Engineering, National Taipei University of Technology, Taipei, Taiwan, Republic of China

<sup>2</sup> Geology Department, Faculty of Science, Al Azhar University, Asyût, Egypt

grains is observed in granitic and andesitic rocks with a minor degree of metamorphism (Duparc et al. 2016). By contrast, a high Ti concentration is observed in basaltic rocks. Magnetite is considered as a suitable target for geochemical studies because of its ability to incorporate many chemical elements in its cubic spinel structure under general geology conditions (Lindsley 1976a, Lindsley 1991a; Rumble 1976; Ghiorso and Sack 1991; Shane 1998; Barnes and Roeder 2001; Richter et al. 2006; Ryabchikov and Kogarko 2006; Reguir et al. 2008). The presence of rare elements in magnetite is an essential indicator of the magnetite source. Many studies in the fields of ore deposits (Dupuis and Beaudoin 2011; Nadoll et al. 2014; Zhang et al. 2020) and sedimentology (Grigsby 1990; Razjigaeva and Naumova 1992; Yang et al. 2009; Duparc et al. 2016) have focused on these rare elements. Iron oxides are the most common heavy minerals (Pettijohn et al. 1987); therefore, analysis of their sedimentary provenance is essential to identify the iron oxide source. Spinel elements, including Fe, Al, Ti, Mg, Mn, Zn, Cr, V, Ni, Co, and Ga, are commonly substituted with spinel supergroup elements. These elements can replace cations on the A and B sites in magnetite crystals (Lindsley 1976b; Ghose et al. 1977; O'Neill and Navrotsky 1984; Wood et al. 1991; Broughm et al. 2017; Deditius et al. 2018; Hu et al. 2020). Hence, the high average concentrations of elements such as Al, Ti, Mg, Cr, Ni, Mn, and Zn may result in the formation of magnetite crystals through either of the seven mechanisms: the substitution of  $\text{Fe}_2^{3+}$  with  $\text{Al}_2^{3+}$  at magnetite results in the formation of hercynite, gahnite, corundum, spinel, and galaxite; the depletion of  $\text{Fe}_2^{3+}$  at hematite and the subsequent incorporation of  $\text{Ti}^{4+}$  at the hematite structure can lead to ulvöspinel formation, or the substitution of  $\text{Fe}_2^{3+}$  with  $\text{Ti}^{4+}$  can result in ilmenite formation; the substitution of  $\text{Fe}^{2+}$  with  $\text{Mg}^{2+}$  at magnetite results in magnesiochromite and magnesioferrite formation; the substitution of  $\text{Fe}_2^{3+}$  with  $\text{Cr}^{4+}$  at magnetite results in magnesiochromite and chromite formation; the substitution of  $\text{Fe}^{2+}$  with  $\text{Ni}^{2+}$  at magnetite leads to trevorite formation; the substitution of  $\text{Fe}^{2+}$  with  $\text{Mn}^{2+}$  results in galaxite and jacobite formation and  $\text{Fe}_2^{3+}$  by  $\text{Mn}_2^{3+}$  leads to bixbyite formation; and the substitution of  $\text{Fe}^{2+}$  with  $\text{Zn}^{2+}$  leads to gahnite and franklinite formation. These elements can be used for easily distinguishing magnetite from different sources (Rusk et al. 2009). Various trace elements have been determined at sub-ppm levels through laser ablation inductively coupled plasma mass spectrometry (LA-ICP-MS). Ti, Mn, Cr, V, Ni, Co, Zr, Sn, Zn, Pb, and Cu concentrations can be used to trace the source rocks of sediments (Razjigaeva and Naumova 1992).

Since the origin of Fe mineralization, especially magnetite, remains controversial, the sources of magnetite and other ore materials can be inferred based on the

geochemistry of magnetite, which exerts direct constraints on the sources. Although many studies have examined the chemistry of magnetite minerals in other countries (Nadoll et al. 2012, 2015; Pisiak et al. 2017; Salazar et al. 2019; Zhang et al. 2020), no study on this topic has been conducted in Taiwan. Therefore, the main purposes of this study were as follows:

- (1) To construct a magnetite distribution map.
- (2) To determine the provenance of magnetite using a discrimination diagram and to detect the type of the studied magnetite. Here, we examined the provenance of magnetite found in northern Taiwan (the present study). In our next study, we will determine the source of magnetite found in the eastern and western parts of Taiwan. In the future, we will compare the chemical composition and provenance of magnetite present in whole Taiwan with those of some historical mineral materials made of iron in the Shihsheng Museum of Archeology to determine if the source of iron of these mineral materials is the same as the ore of Taiwanese magnetite iron.
- (3) To examine the presence of other mineralization types associated with magnetite by determining the concentration of trace elements belonging to the spinel group.

## 2 Geological setting

The study area extended over 135 km and is located in north Taiwan between a longitude of  $120^\circ 52' 24.1''$  and  $122^\circ 05' 51.88''$  E and latitude of  $24^\circ 45' 26.07''$  and  $25^\circ 22' 14.45''$  N (Fig. 1). The study area consists of five large regions: Hsuehshan Range (HR) and Western Foothills (WF) in the south and east, respectively; Tatun Volcano Group (TV) in the north; Linkou Tableland (LT) in the west; and Taoyuan Tableland (TT) in the west. These five regions mainly consist of the following rock types: HR formed from Kankou and Tatungshan formations (argillite, sandy shale, slate, and sandstone); WF formed from Jui-fang and Yehliu groups (sandstone and shale); TV and LT formed from andesite, volcanic agglomerate (breccia; andesitic pyroclastics), and some basalt; and TT formed from lateritic terrace deposits (laterite, gravel, sand, and clay) and alluvium deposits (Fig. 1). TV belongs to the Pliocene–Pleistocene age (Chen and Wu 1971; Song et al. 2000).

The Tatun region contains a volcano-sedimentary basement as andesitic pyroclasts overlain by volcano lava (Chen and Wu 1971). This region is cut by the Chin-Shan fault, thus dividing these rocks into two parts: the first part is the deformed strata belonging to Oligocene–Lower

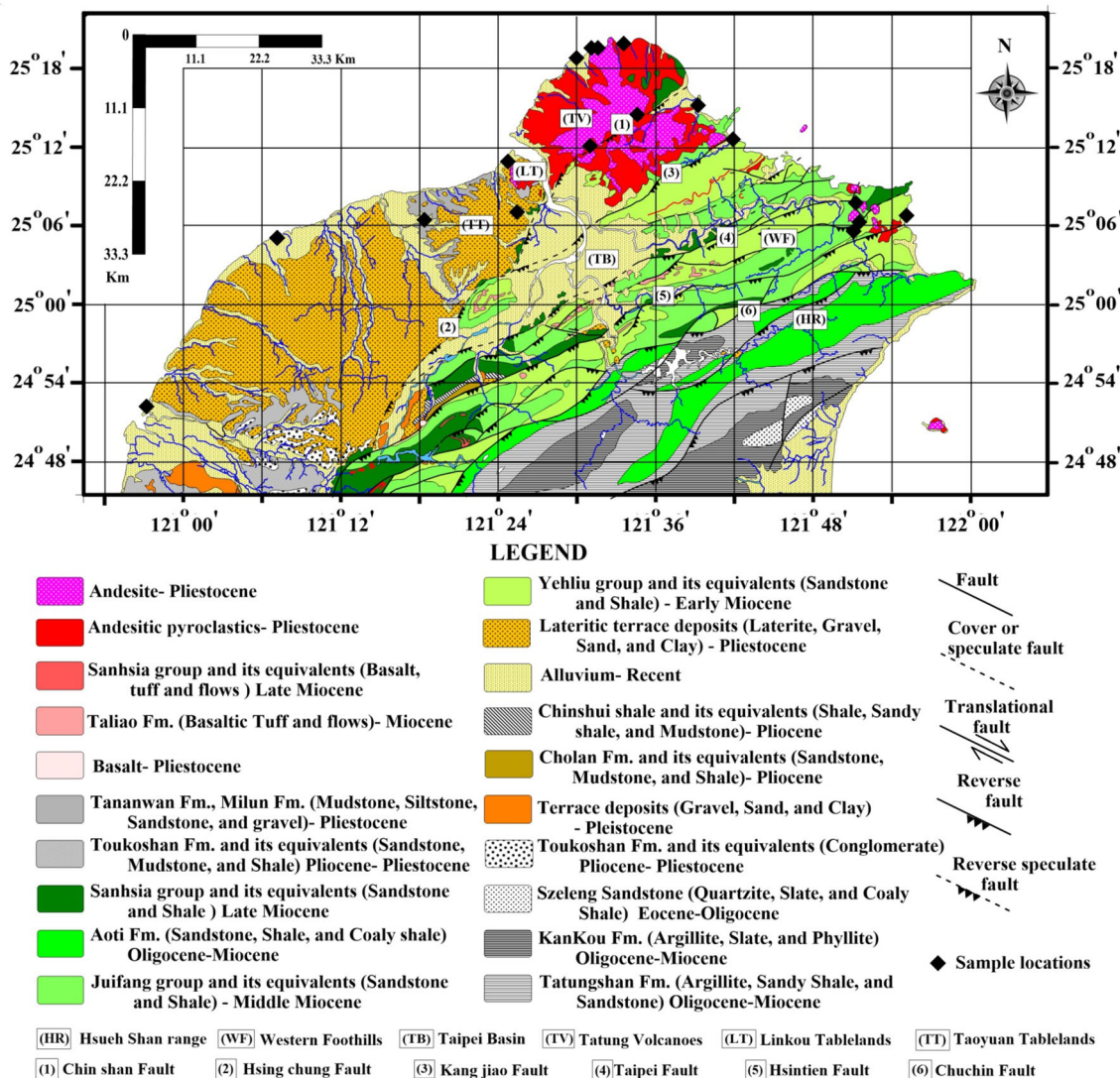


**Fig. 1** Geological map and location of the study area (modified after Lin and Chen (2016))

Miocene on the southeast side (Ho 1983; Yen et al. 1984), and the second part is the dissected terrace of LT with 220–250 m of its height being covered by lateritic soil and underlain by the conglomerate, sandstone, and mudstone of Pliocene–Pleistocene. In addition, the dissected terrace of LT is covered by basaltic rocks similar to those found in TV (Chen 1989; Hwang and Lo 1986; Tien et al. 1995), and the eastern edge is cut by the Shangjiao fault (Tan 1939; Chen 1953; Lin 1957). Several faults affect the study area (Fig. 1), namely (1) Chinshan, (2) Hsingchung, (3) Kangjiao, (4) Taipei, (5) Hsintien, and (6) Chuchin (Teng et al. 2001).

## 2.1 Sample collection and preparation

The studied samples were collected from different places in northern Taiwan (Fig. 1). Figure 2 shows the field sample

collection and analytical methods used in this study. Twenty-three samples were collected from various sites (eight samples from stream sediments, eight samples from rugged rocks around the streams, and seven samples from the beach sand; Table 1 in Supplementary Information). We can observe the thickness of the magnetite beds for the beach sand ranged from 2 to 3 cm (Fig. 3). These samples were prepared using mixed methods. For the analysis of magnetite, rock samples were prepared by selecting certain places in the rocks found on some of the magnetite crystals and then cutting rocky slides with an electric saw (1 cm × 1 cm × 2 mm). Subsequently, only one side was polished to examine magnetite under a measuring microscope. Finally, the prepared samples were observed through scanning electron microscopy (SEM) and LA-ICP-MS.



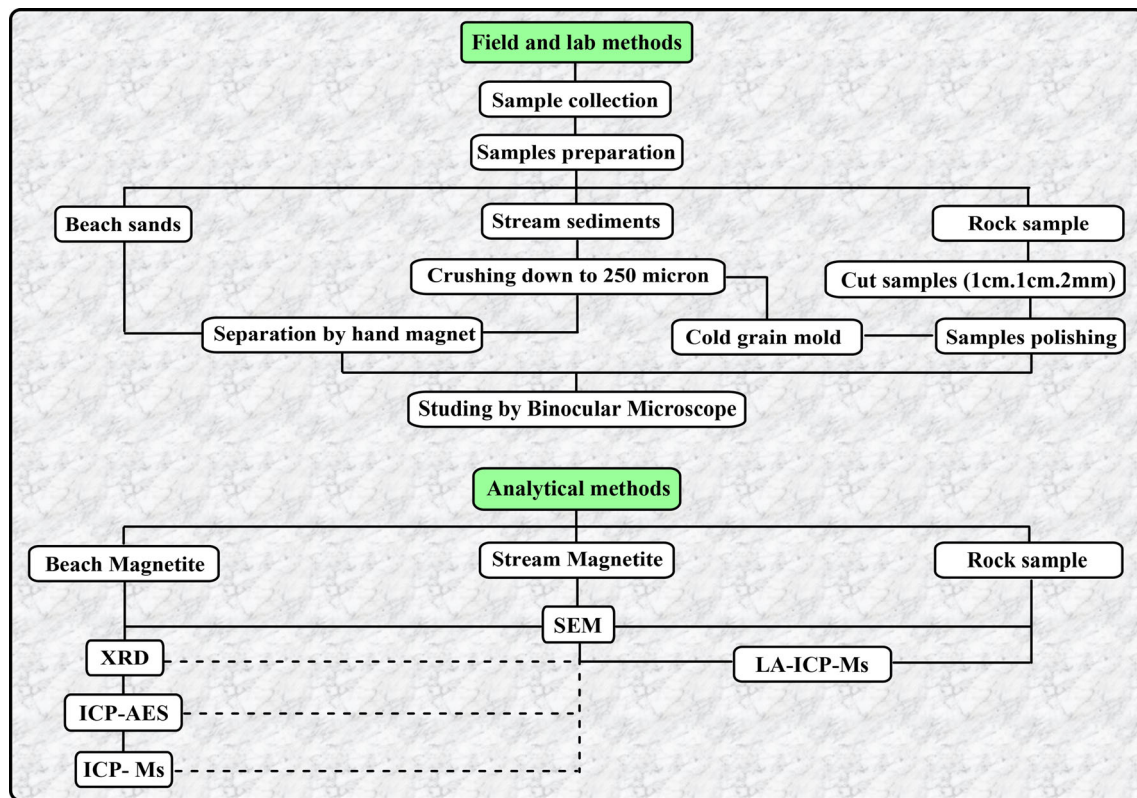


**Fig. 2** Field and lab operations and analytical methods

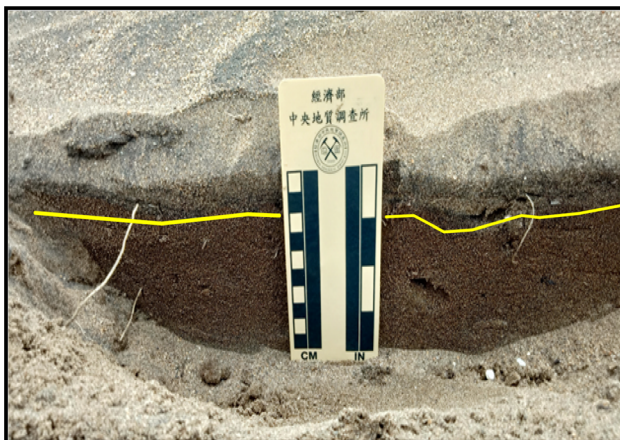


**Fig. 3** Thickness of magnetite-bearing beach sands

Stream samples were obtained by collecting a quantity of sand lying at the bottom of the stream. We observed that magnetite crystals were coherently intertwined with some other grains such as quartz grains and fibers. Thus, to minimize the size of granules, we crushed the samples to a size of approximately 250  $\mu\text{m}$ . This process enabled us to obtain a substantial number of magnetite crystals and to separate magnetite crystals from quartz grains and fibers. Subsequently, the samples were separated using a handheld magnet with a low magnetic field. In addition, we hand-

picked the samples to prevent the attraction of other metals to magnetite. Since the magnetite amount was considerably limited, SEM and LA-ICP-MS were performed; only three samples were adequately large to be analyzed through inductively coupled plasma atomic emission spectroscopy (ICP-AES) and inductively coupled plasma mass spectrometry (ICP-MS). We realized that the pure magnetite grains in the beach samples were up to 60 mesh in size. In the next section, the sample preparation methods used in this study are described in detail.

### 3 Analytical methods

A measuring microscope (Olympus STM7-SFA) was used to examine the purity of the studied magnetite grains. This measuring microscope was attached to a PC at the National Taipei University of Technology. The magnetite grains in the beach samples, individual grains in the stream samples, and rock slices were evaluated using this microscope. The purity of magnetite grains in the beach sand and some of the stream sediments was tested through X-ray diffraction (XRD; Figs. 4, 5) performed using a D2 instrument with a scintillation counter (NaI scintillator coupled with a photomultiplier with a preamp); the parameters were as follows: a rated output of 2200 V at 3 kW, a Cu-target tube, a



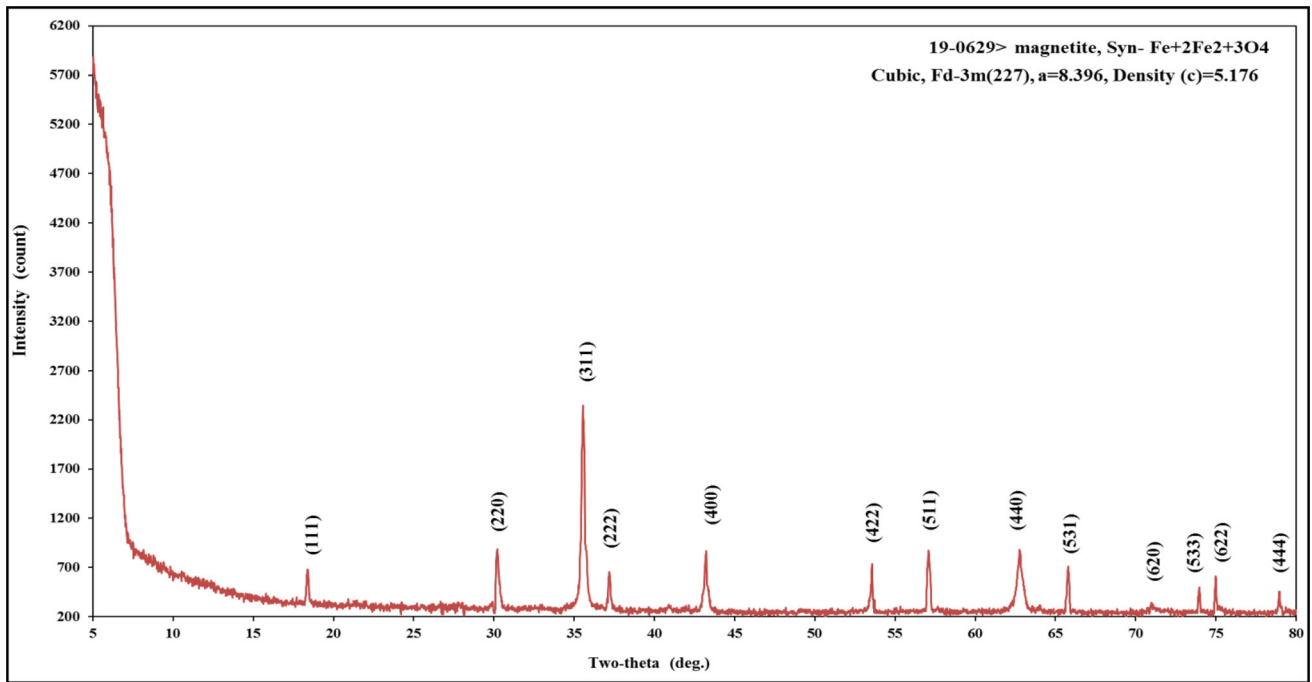


**Fig. 4** XRD patterns of magnetite at stream sediments in White Sand Bay Creek

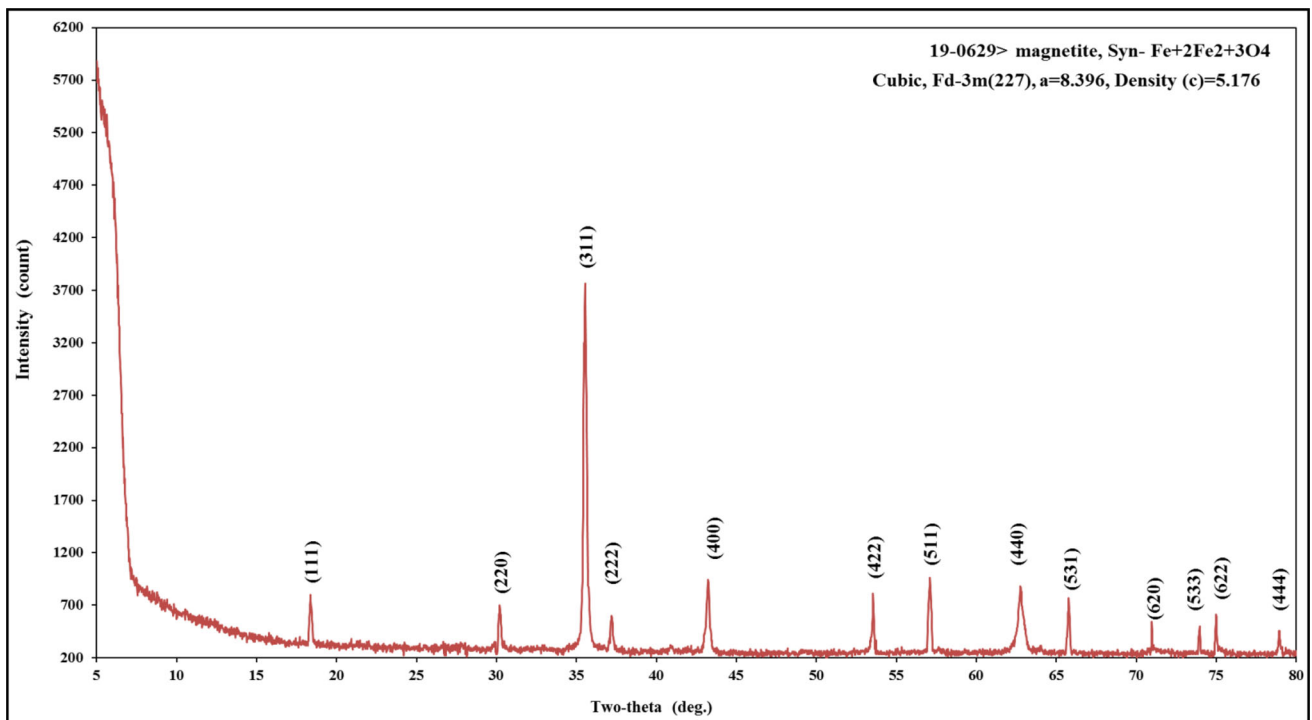


**Fig. 5** XRD patterns of magnetite at beach sand in White Sand Bay Beach

Ni filter at 40 kV and 30 mA, a start angle of  $5^\circ$ , a stop angle of  $70^\circ$ , and a scan speed of  $2.00^\circ \text{ min}^{-1}$ . The XRD commander and measurement server were connected to the D2 instrument to obtain XRD patterns. Jade software was used for mineral identification in the XRD Laboratory at

the National Taipei University of Technology. Approximately 5 g of each sample was ground to a grain size of  $< 270$  mesh. An appropriate amount of the ground sample was placed in the middle of the holder; the sample

surface was flattened, and a slide was used to scrape off excess powder around the small circle.

The stream and beach sample molds and rock magnetite slices were coated with Au and C by using the JFC-1600 Auto Fine Coater. The SEM instrument JSM-6510 was used to obtain back-scattered electron (BSE) images for determining the chemical composition of elements at the SEM Laboratory in the National Taipei University of Technology. The operation conditions were as follows: acceleration voltage, 15 kV; 20 nA; acquisition time, 60 s; and spot size, 50  $\mu\text{m}$ . The samples used for SEM were collected from beaches, streams, and rock slices, as described previously. Magnetite was examined in the polished rock slides with dimensions of 1 cm  $\times$  1 cm  $\times$  2 mm. After the magnetic separation of the samples, some grains were separately selected and placed in a plastic mold lined with Vaseline. Epofix resin and Epofix hardener were mixed at a ratio of 7:1. This mixture was poured into the plastic mold on magnetite grains to form a thick layer (approximately 1 or 1.5 cm). The molds were placed in an oil-less vacuum pump device to remove air from the mixture for 5–7 min. Subsequently, the samples were dried for more than 24 h. Finally, the epoxy mold was polished using sandpapers of different sizes.

Many chemical analyzers were used in this study for several reasons. Because most of the stream samples were not available in large quantities, the amount of magnetite obtained after its separation from other accompanying minerals in stream sediments was not adequate to be analyzed through ICP-MS and ICP-AES, which require a considerable amount of a sample to prepare a solution. Generally, REE solution (1000  $\mu\text{g mL}^{-1}$ ) with high purity (99.9%; stock solution) is dissolved in hot nitric acid and then diluted with deionized water to 50 mL. The REE standard working solution used for ICP-AES calibration was prepared using 34.12 mL of nitric acid and 15.88 mL of distilled water. This acid solution was maintained at a temperature of 70  $^{\circ}\text{C}$  for 1 h during the reaction process. A glass lid was placed on the beaker to prevent rapid evaporation. A thermometer was used to measure whether the temperature of the solution in the beaker reached 70  $^{\circ}\text{C}$ . The stirrer's temperature was readjusted to 145  $^{\circ}\text{C}$ . Subsequently, the sample powder was added, and the solution was stirred for 24 h. The prepared acid solution was filtered and stored in polyethylene bottles. Five diluted standard solutions (10, 5, 2, and 1 ppm) were prepared using a stock solution with a concentration of 1000  $\mu\text{g mL}^{-1}$ . Trace and rare earth elements were analyzed using ICP-AES (iCAP 7000) at the Institute of Mineral Resources Engineering in National Taipei University of Technology under the following conditions: argon pressure cylinder, 90 psi; nebulizer gas flow, 0.50  $\text{L min}^{-1}$ ; coolant gas flow, 12  $\text{L min}^{-1}$ ; ciliary gas flow, 0.5  $\text{L min}^{-1}$ ; pump speed, 50 rpm; axial

measure mode; manual fast injection time (uptake time), 30 s; and wash time, 10 s. The chemical composition of magnetite was examined using the ICP-MS instrument in Canada-Vancouver Lab (Mineral Laboratories, Bureau Veritas Commodities Canada, Ltd.). The samples were subjected to an extra wash with silica and pulverized to 85% by passing them through a 200-mesh screen. A 0.25 g of the split powder was heated in  $\text{HNO}_3$ ,  $\text{HClO}_4$ , and HF to fuming; dried in tightly sealed 25-mL Teflon perfluoroalkoxy screw-cap beakers, and finally heated for 1 day on a hot plate at 130  $^{\circ}\text{C}$ . The decomposed sample was placed inside an oven for evaporation and subjected to 120  $^{\circ}\text{C}$  for 24 h, 160  $^{\circ}\text{C}$  for 6 h, and 190  $^{\circ}\text{C}$  until dryness. Subsequently, aqua regia was added to the residue; the mixture was heated at 130  $^{\circ}\text{C}$  for 12 h and evaporated. Approximately 5 mL of HCl was used to dissolve the residue to form the solution. The solution was diluted to 100 mL as the total volume.

Many elements can be analyzed with high precision at a low detection limit (ppm) through LA-ICP-MS. We used a laser ablation system (GeoLasPro HD; Wuhan Shangpu Analytical Technology, Co., China) that had a resolution of 193 nm and was coupled with Agilent 7900  $\times$  ICP-MS. A beam size of 30  $\mu\text{m}$ , a stage speed of 3.5  $\text{lm s}^{-1}$ , a laser frequency of 5 Hz, and an energy density of approximately 5  $\text{J cm}^{-2}$  were used during the analysis. High-purity helium (650  $\text{mL min}^{-1}$ ) and makeup gas (Ar; 0.8–0.9  $\text{mL min}^{-1}$ ) were introduced into the ablation cell. NIST 640, BHVO-2G, BIR-1G, and BCR-2G were used to calibrate magnetite for all elements, except for P, which was calibrated using GSD-1 g (Nadoll and Koenig 2011). All the analyzed reference materials yielded accurate results within a standard deviation of < 5%. The magnetite concentrations were determined using Iolite software (Patton et al. 2011). The samples analyzed using SEM were also subjected to LA-ICP-MS.

## 4 Results

Using the magnetite grains found in the beach sand and stream sediments (Table 2 in Supplementary Information), we constructed a distribution map of magnetite in north Taiwan (Fig. 6). In the far north of Taiwan, especially in the areas of Wanli, Fengyu, Laomei, White Sand Bay Creek, White Sand Bay Beach, and Xinzhuangzi, high concentrations of magnetite were found. The magnetite concentration exhibited a decreasing trend toward the northeast direction and was lower concentration in Longdong Bay, Keelung Mountain, Wudang Shan, and Chin-Kuashih Penshan Geological Park Creek regions. In addition, the magnetite concentration exhibited a decreasing trend toward the northwest direction in the areas

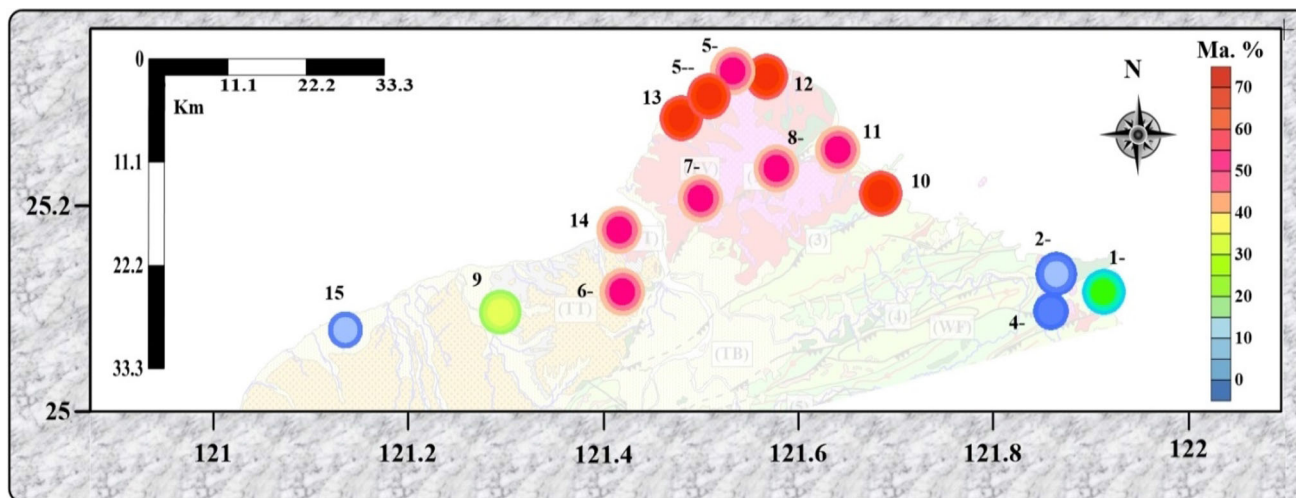


**Fig. 6** The magnetite distribution map in north Taiwan

Qingshan Waterfall, Cai Gongkeng Creek, Bianshan Fuan Palace Creek, and Shisan Hun, and it was a low concentration in Bianshan Fuan Palace Creek. The magnetite concentration gradually increased and reached an average value in Linkou Creek, decreased toward the direction of the Guanyin region, and then increased again in the Crescent Beach region. In most areas in (1) White Sand Bay Creek, Wanli fishing port seaside, and Laomei; (2) Xinzhuangzi; and (3) White Sand Bay Beach, Fengyu, and Cai Gongkeng Creek, the magnetite content in the beach sand and stream sediments ranged from 50 to 70% (Table 2 in Supplementary Information). This finding supported our speculation that the magnetite found in the beach sand and stream sediments are of economic value. Under a measuring microscope, the magnetite present in the beach sediments was observed as black to silvery gray grains with high magnetic character. Magnetite occurred as octahedral crystals with metallic to submetallic luster (Fig. 7A). The size of the magnetite present in these sediments ranged from 0.04 to 0.09 mm. Magnetite grains found in the rock samples were subdivided into two major classes based on their intergrowth morphology: homogeneous grains (Fig. 7B) observed in BSE images (Fig. 7D) usually containing one mineral and grains containing more than two elements (Fig. 7C) exhibiting a light-pink intergrowth in magnetite in BSE images (Fig. 7E); the incorporated element Ti oxide was detected on the basis of EDX peaks (Fig. 7F). Based on SEM and EDX peaks, the chemical elements of magnetite in the beach, stream, and rock samples were determined (Table 3 in Supplementary Information; Figs. 1, 2, 3 in Supplementary Information). The Fe and Ti content ranged from 77.8% to 56.1% and from 6.4% to 1.7%, respectively. The chemical composition of magnetite grains present in the beach, stream, and rock samples was analyzed through LA-ICP-MS (Tables 4,

5, 6 in Supplementary Information). The results of LA-ICP-MS were considerably similar to the average results of magnetite grains in the beach samples and some stream samples obtained using ICP-MS (Table 7 in Supplementary Information) and ICP-AES (Table 8 in Supplementary Information). Furthermore, the results of ICP-MS and ICP-AES were similar, but the results of ICP-AES differed from those of LA-ICP-MS. We used these results in the interpretation and discussion of the chemical composition of magnetite.

In terms of the chemical composition, we compared the average results of the analyzed beach, stream, and rock magnetite samples with those in studies conducted in different parts of the world (Table 9 in Supplementary Information). The concentrations of Ti, Al, Mg, Sc, V, Cr, Mn, Co, Ni, Cu, Zn, Ga, Sn, Nb, Hf, and Ni/Cr found in our samples were considerably similar to the magnetite composition of andesite rocks reported by Dare et al. (2014). This finding indicates that the magnetite samples examined in the present study may have originated from surrounding andesite rocks. The plot of Ti (ppm) versus the Ni/Cr ratio (nonnormalized) in magnetite provided by Dare et al. (2014) was used to differentiate between magmatic and hydrothermal origins (Fig. 8A). The results of the chemical analysis revealed that magnetite was present within the field of magmatic magnetite; this finding is in contrast to previous findings obtained through EMP and LA-ICP-MS for mafic, felsic, and intermediate rocks (Razjigaeva and Naumova 1992); basalt (Gregory 2006); andesite (Chiariadia et al. 2011); and felsic plutonic (Nadoll et al. 2012, 2014; Park et al. 2013; Dare et al. 2014). According to the method of Dupuis and Beaudoin (2011), the chemical composition of magnetite was determined by plotting the Ni/(Cr + Mn) versus Ti + V and Ca + Al + Mn versus Ti + V discriminant diagrams (Fig. 8B, C). The



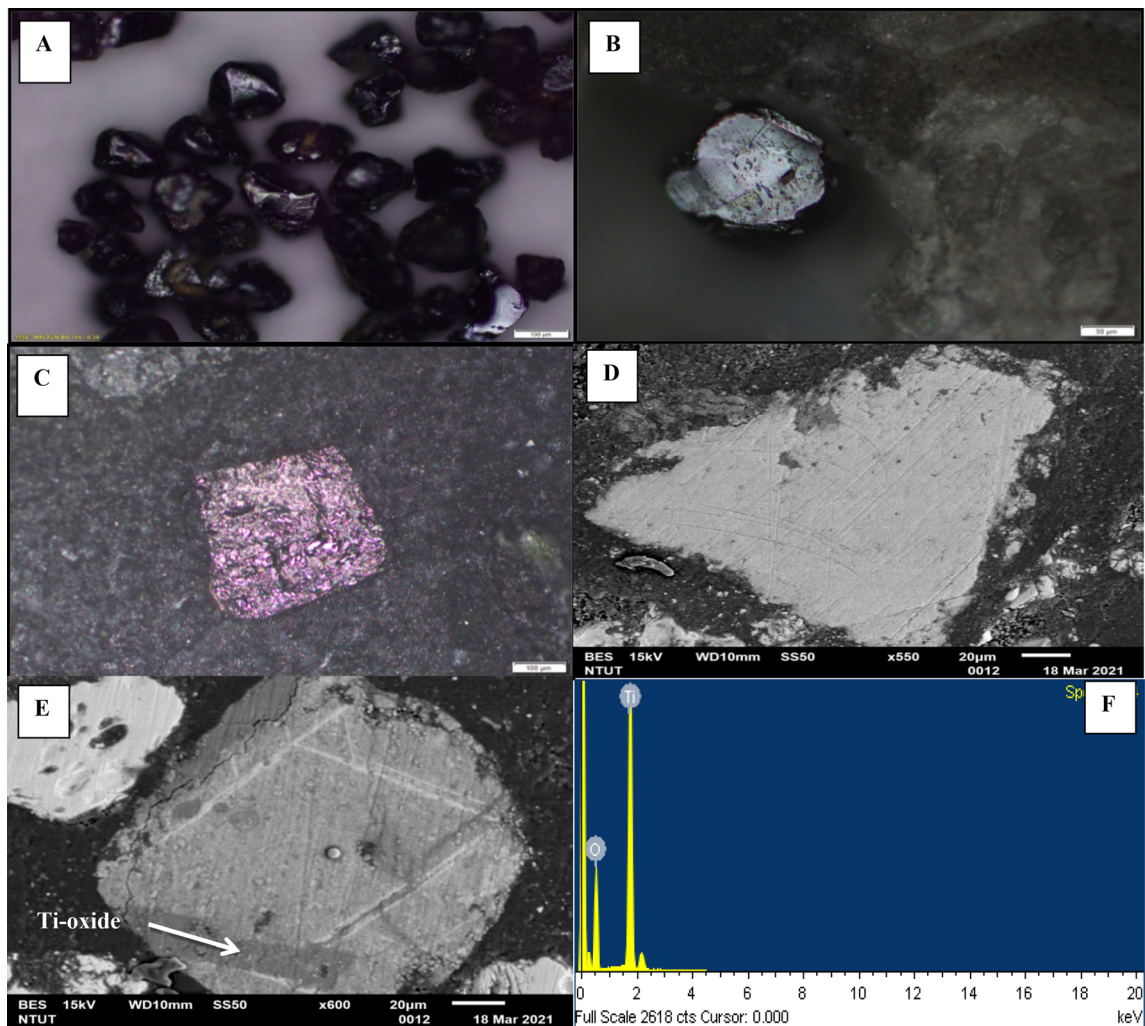


**Fig. 7** Magnetite grains observed under a measuring microscope (A–C), BSE images (D and E), and EDX peak (F)

types of the magnetite environment could be detected using these diagrams including Kiruna, iron oxide–copper–gold (IOCG), porphyry Cu, Fe–Ti–V, and banded iron formation (BIF) fields. As shown in Fig. 8B, C, all the samples were plotted in the Fe–Ti–V field. The chondrite-normalized diagrams (Fig. 8D–F) plotted to characterize the REE distribution pattern in the stream, beach, and rock magnetite samples were compared with the chondrite values reported by Taylor and McLennan (1985). The general trend of the enrichment of REEs in the stream, beach, and rock magnetite samples indicated that REEs gradually decreased from La–Lu with a considerable decline in Y, Gd, and Lu, indicating higher enrichment of light REEs than that of heavy REEs (Fig. 8D–F). However, an increase in the enrichment of Tm and Lu was observed in the beach and rock magnetite samples (Fig. 8E, F). A substantial increase in Tm was noted in the rock magnetite samples collected from localities such as Cai Gongkeng, Wudan Mountain, Qingshan Waterfall (Dagu Mountain),

and Bianshan Fuan Palace (Guanyin Mountain; Fig. 8F). Generally, the enrichment of REEs increased with a decrease in the atomic radius and an increase in the atomic number.

The magnetite data normalized to the bulk continental crust of Taylor and McLennan (1985) and plotted on Dare et al.'s (2014) multielement variation diagram to expect the liquid's original composition in which magnetite was formed. We chose the bulk continental crust because its composition is closer to that of an evolved silicate melt (saturated in magnetite) than that of the primitive mantle (undersaturated in magnetite), and hydrothermal fluids are more likely to interact with crustal rocks rather than the primitive mantle. The normalized patterns of the magmatic magnetite present in the stream, beach, and rock grains (Fig. 9) increased from the left (lower values for elements incompatible with magnetite) to the right (higher values for elements compatible with magnetite). Some elements, namely Al, Cu, Ga, Hf, and Zn (Fig. 9A–C), consistently

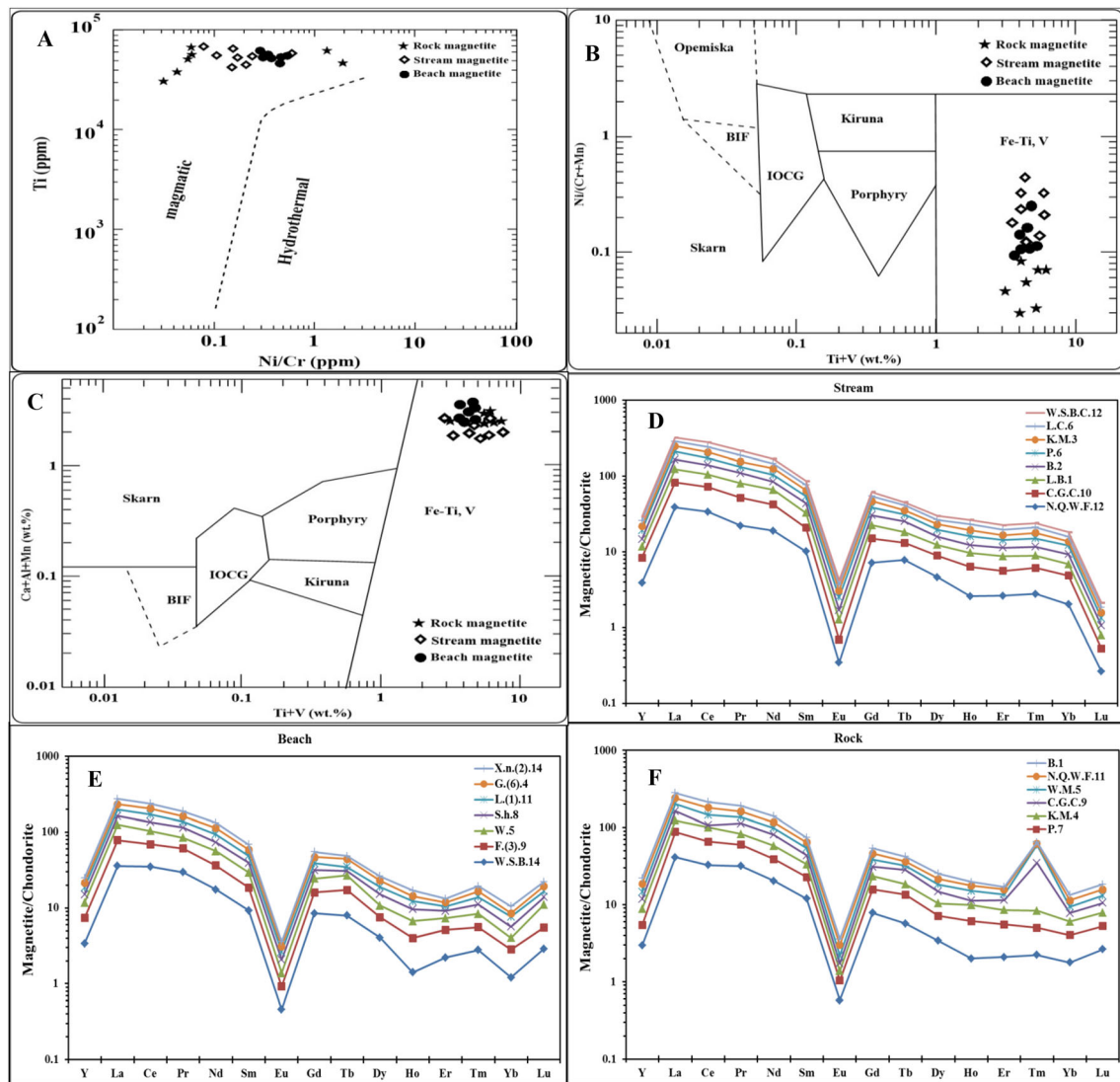


**Fig. 8** **A** Ni/Cr vs. Ti diagram dividing the genesis of magnetite to magmatic and hydrothermal (Dare et al. 2014), **B** Ni/(Cr + Mn) vs. Ti + V and **C** Ca + Al + Mn vs. Ti + V discriminant diagrams constructed to determine the type of the magnetite environment, namely Kiruna, IOCG, porphyry Cu, Fe–Ti–V, and BIF (Dupuis and Beaudoin, 2011), and **D–F** chondrite-normalized REE diagram for the stream, beach, and rock magnetite samples, respectively

exhibited the highest magmatic magnetite concentrations in the stream, beach, and rock samples. Most elements, including Zr, Sc, Ta, Nb, Cu, Mo, Sn, Mn, Mg, Ti, Co, V, Ni, and Cr, consistently exhibited the lowest concentrations. The concentrations of Ca, Y, Pb, and W are the same as those reported by Dare et al. (2014). Thus, any difference in the shape of the magnetite pattern would reflect the abundance of different trace elements in the liquid. The composition of magnetite obtained from environments with similar physiochemical conditions would be identical. By contrast, the composition of magnetite formed under different conditions would be distinct, thus resulting in distinctive chemical signatures that can aid in the differentiation of magnetite obtained from different

environments (Dupuis and Beaudoin 2011; Nadoll et al. 2014). Thus, the elements incompatible with magnetite exhibited the same trend in the stream, beach, and rock samples (Fig. 9A–C); this finding indicates that the source of magnetite present in the stream and beach samples is the same as that of magnetite present the rock samples.

Al demonstrated a negative correlation with Fe. Ti, Ni, Cr, V, Co, Mo, Nb, Ga, Sn, and Ta exhibited a positive correlation with Fe but a negative correlation with Al. Furthermore, Mg, Ca, Li, Sc, Mn, Cu, Zn, As, Rb, Sr, Y, Cd, Sb, Cs, Ba, REE, Pb, U, and Th exhibited a negative correlation with Fe and a positive correlation with Al (Table 10 in Supplementary Information). Elements exhibiting significant variations in magmatic magnetite

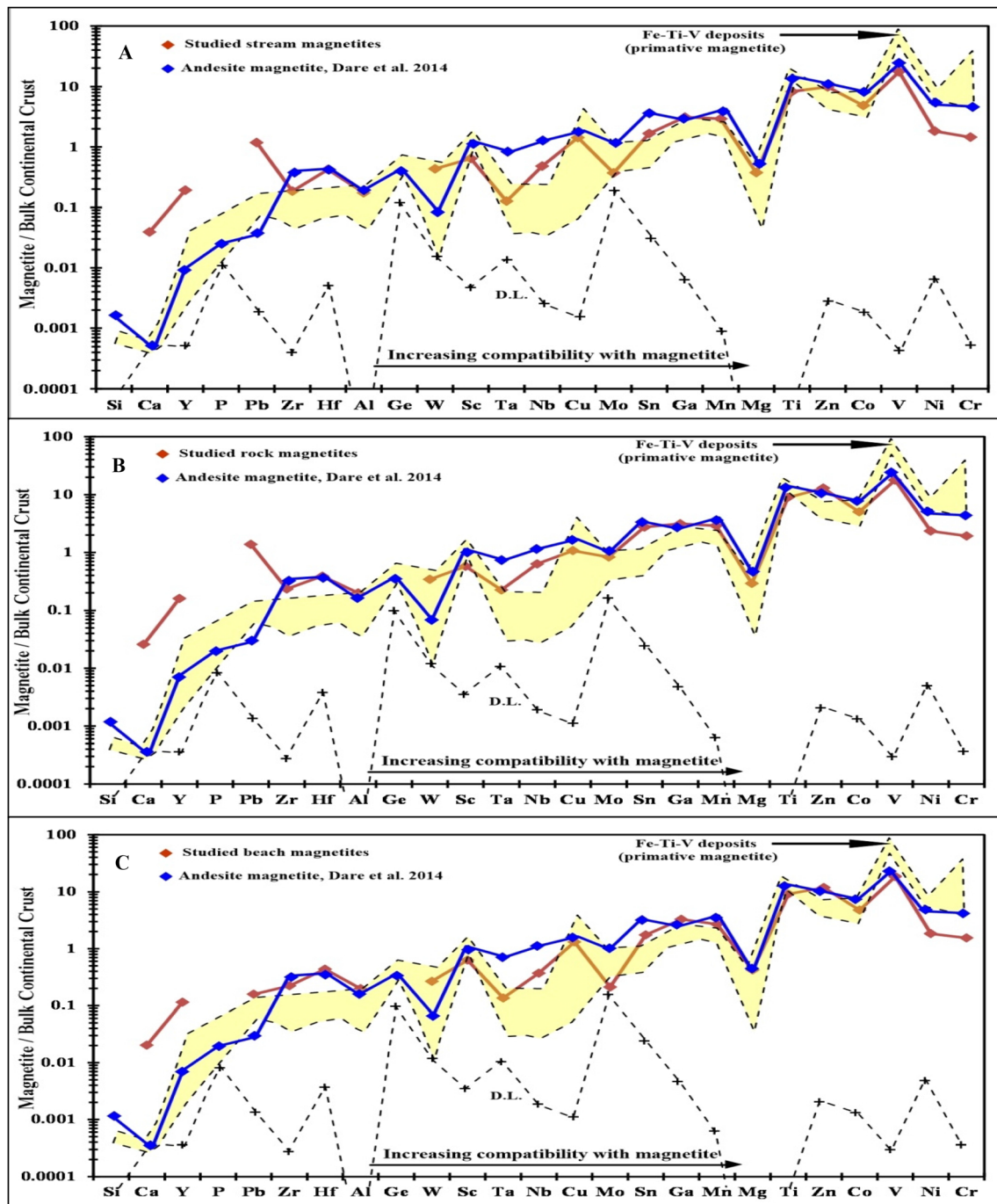


**Fig. 9** Multi-element variation diagrams developed by Dare et al. (2014) were used to determine the liquid's original composition of formed magnetite normalized to Taylor and McLennan's bulk continental crust (1985). The yellow field is a magmatic magnetite field from intermediate magmas (Greenfield, Bushveld Complex, and South Africa) (Dare et al. 2014). The blue refers to andesitic magnetite reported by Dare et al. (2014), and the red line refers to the **A** stream, **B** beach, and **C** rock magnetite samples

between localities are summarized in median and quartile plots (Fig. 10). We observed considerable similarity in the elements' behavior for the stream, beach, and rock magnetite samples (Fig. 10; Tables 11, 12, 13 in Supplementary Information). These aforementioned chemical elements were categorized into five groups depending on

their concentrations: Al, Mg, V, Mn, Ca, P, and K (> 1000 ppm); Na, Cr, Ni, Cu, and Zn (between 1000 and 100 ppm); Co, Sc, Ga, Zr, Sr, and Ba (between 100 and 10 ppm); Y, Nb, Sr, La, Ce, Pr, Sm, Dy, and Rb (between 10 and 1 ppm); and Er, Yb, Hf, Ta, Th, U, Ag, Cd, Sb, Cs,



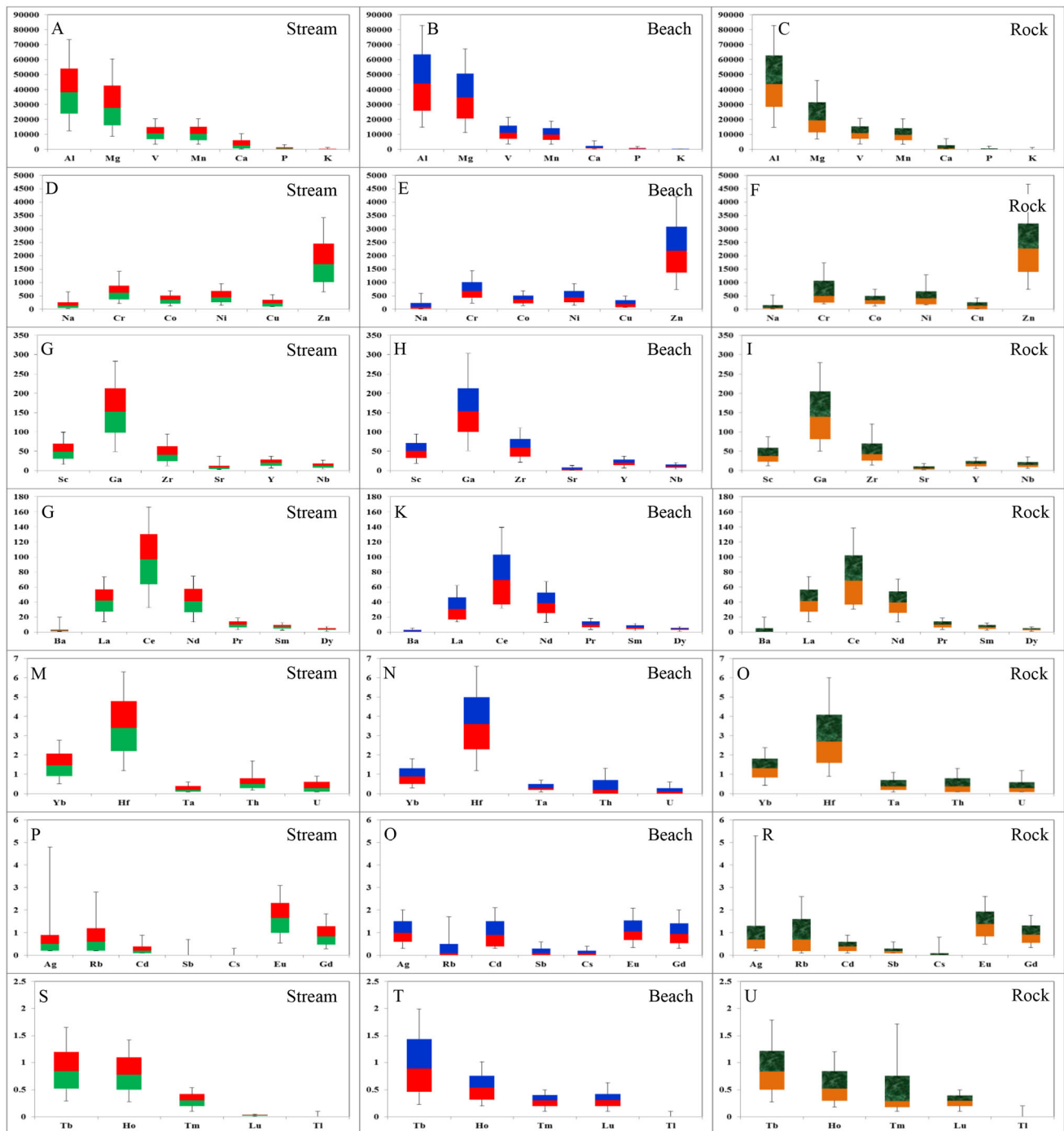


**Fig. 10** Box-and-whisker plots of the most trace and rare earth elements of the stream (A, D, G, J, M, P, and S), beach (B, E, H, K, N, Q, and T), and rock magnetite samples (C, F, I, L, O, R, and U). The box encompasses the median (line) and is bounded by the upper and lower quartiles

Eu, Gd, Tb, Ho, Tm, U, and Tu (< 0.1 ppm; Tables 11, 12, 13 in Supplementary Information; Fig. 10A–U).

## 5 Discussion

### 5.1 Type and origin of the magnetite

The formation of magnetite deposits can be explained using three genetic models: (1) crystallization from iron-

rich melts that were immiscible from the parental silicate melt and were emplaced at different depths or erupted and crystallized at the surface where crystallization was accompanied by the exsolution of large amounts of magmatic–hydrothermal fluids (Henríquez and Martin 1978; Nyström and Henríquez 1994; Naslund et al. 2002; Alva-Vadivia et al. 2003; Nyström et al. 2008; Martinsson et al. 2016; Tornos et al. 2016); (2) replacement of host rocks with iron-rich hydrothermal fluids (Hitzman 2000; Edfelt et al. 2005; Groves et al. 2010; Dare et al. 2015); and (3) magmatic–hydrothermal genesis (Knipping et al. 2015). Although Parák (1975) suggested a sedimentary origin; the suggestion was not accepted (Frietsch 1978; Nyström et al. 2008). Using LA-ICP-MS, Dare et al. (2014) examined trace elements in magnetite as petrogenetic indicators. They developed a diagram to determine magnetite genesis by defining fields (magmatic and hydrothermal). By using this diagram, the studied samples were determined to be present within the magmatic field. This result was confirmed by Duparc et al. (2016), who reported that magnetite from felsic magmas contained a low Ni/Cr ratio. Dupuis and Beaudoin (2011) investigated the trace element concentration of magnetite obtained from various mineral deposits by using an electron microprobe. They developed discrimination diagrams for the different sources of magnetite. They defined the following fields of the magnetite environment based on the concentrations of Ti, V, Ni, Cr, and Mn in magnetite: Kiruna, IOCG, porphyry Cu, Fe–Ti–V, and BIF. Using the aforementioned two diagrams, we observed that the studied samples were present within the Fe–Ti–V field. Therefore, the field of magnetite determined in this study is similar to that of Fe–Ti–V–P deposits hosted by mafic–ultramafic layered intrusions (Bushveld Complex, South Africa, and Sept Iles, Canada) (Dare et al. 2012a, b). This can be related to the fact that the concentration of an element in magnetite depends on (a) the concentration of the element in the liquid form which it crystallizes, (b) whether other minerals crystallizing at the same time are competing for that element, and (c) the partition coefficient (D) of the element in magnetite, which can vary up to several orders of magnitude based on the composition of the silicate melt, temperature, pressure, oxygen fugacity ( $fO_2$ ), and cooling rate (Mollo et al. 2013; Nadoll et al. 2014). In particular, Ti and V concentrations in magnetite progressively increase with the temperature of original magma (Buddington and Lindsley 1964; Waychunas 1991). The temperature contributes to the increase in Ti and V concentrations; at temperatures above 600 °C, a continuous solid solution exists between magnetite and titanomagnetite ( $Ti_xFe_{3-x}O_4$ ) (Buddington and Lindsley 1964; Waychunas 1991). The partition coefficient of magnetite/liquid for V increases with a decrease in  $fO_2$ ; therefore, at low  $fO_2$ , vanadium is compatible with

magnetite. Emplacement of andesitic volcanic rocks in the Tatum area marks the onset of Ryukyu arc magmatism and the flipping of subduction polarity (Teng et al. 1992). When the subduction polarity flipped beneath northeastern Taiwan in the Late Quaternary period, collisional orogeny ceased, and Tatum volcanism commenced. Volcanism thrived in Tatum and Kuanyinshan areas, resulting in piles of andesitic cones (Louis et al. 2001). During the subduction process, water-saturated magma nucleates bubble on magnetite grains, which intrude into the base of the andesite magma body, resulting in the accumulation of magnetite crystals at the andesite magma (Edmonds et al. 2015). Although no such deposits were noted in the studied region, such deposits might exist in the surrounding region. The similarity in the chemical composition of the studied samples and Fe–Ti–V deposits can be considered a clue for further geological prospecting of Fe–Ti–V deposits.

Temperature substantially affects the incorporation of trace elements into magnetite crystals (McIntire 1963; Huang et al. 2013; Nadoll et al. 2014; Knipping et al. 2015; Deditius et al. 2018; Sun et al. 2019). Lindsley (1991), Rapp et al. (2010), Dare et al. (2012a, b), Nadoll et al. (2012), Duparc et al. (2016), and Sun et al. (2019) have reported a positive correlation between the formation temperature and the Ti concentration in magnetite. In this study, the high average Ti concentrations in the stream, beach, and rock magnetite samples (39845.21, 42399.72, and 39382.26 ppm, respectively) suggested an increase in temperature during their formation. Li and Xie (1984), Canil et al. (2016), and Broughm et al. (2017) have reported that magnetite with a higher Ti concentration formed at temperatures > 700 °C. Vanadium can occur in various valence states; therefore, its behavior is strongly linked to  $fO_2$  (Nielsen et al. 1994; Righter et al. 2006). Vanadium has two oxidation states in the natural environment: 3+ and 5+.  $V^{3+}$  has the highest compatibility with the spinel structure of magnetite (Balan et al. 2006; Righter et al. 2006). At high  $fO_2$  and in the 5+ oxidation state, vanadium is incompatible with magnetite. Therefore, the partition coefficient of magnetite/liquid for V decreases with increasing  $fO_2$  (Hu et al. 2020). In our study, the box and whisker plot for vanadium (Fig. 10A–C) showed high V concentrations in the stream, beach, and rock magnetite samples, indicating low  $fO_2$ .

In the chondrite-normalized diagram (Fig. 8D–F), the studied magnetite exhibited a negative europium anomaly. This finding can be attributed to the amount of feldspar fractionation and the oxidation state of magnetite magma formation. Eu has two valence states:  $Eu^{2+}$  and  $Eu^{3+}$ .  $Eu^{2+}$ , but not  $Eu^{3+}$ , is compatible with the plagioclase and K-feldspar crystal structure. Thus, the removal of plagioclase and K-feldspar from magma, particularly felsic magma, through crystal fractionation or partial melting can

result in the Eu anomaly (Rollinson 1993). In the multi-element variation diagram (Fig. 9A–C), we observed that some chemical elements, such as Al, Cu, Ga, Hf, and Zn, consistently exhibited the highest concentration in magmatic magnetite. Most elements consistently demonstrated the lowest magmatic magnetite concentrations, including Zr, Sc, Ta, Nb, Cu, Mo, Sn, Mn, Mg, Ti, Co, V, Ni, and Cr. The concentrations of Ca, Y, Pb, and W in magnetite are the same as those reported by Dare et al. (2014). In addition, we observed that the elements incompatible with magnetite exhibited the same trend for the stream, beach, and rock magnetite samples (Fig. 9A–C). This finding indicates that the stream and beach magnetite had the same source as did the rock magnetite. Titanium is a common element in magnetite and undergoes a coupled substitution,  $2\text{Fe}^{3+} = \text{Ti}^{4+} + \text{Fe}^{2+}$ , at high temperatures in ulvöspinel-magnetite solid solutions (Buddington and Lindsley 1964). In fluids, titanium is insoluble, and its concentration in the magma composition is controlled only by temperature (Mysen 2012). Ti-rich magnetite is crystallized before or simultaneously as ilmenite under relatively oxidizing conditions (Toplis and Carroll 1995; Toplis and Corgne 2002; Namur et al. 2010). Both Ti and Al in the magnetite structure exhibited positive temperature dependence (Turnock and Eugster 1962; O'Neill and Navrotsky 1984). Experimentally produced magnetite in felsic igneous rock bulk compositions crystallized at temperatures above 700 °C contained higher concentrations of Ti (10,000 ppm) and Al (4000 ppm) (Canil et al. 2016). The high average concentrations of Ti (39845.21, 42399.72, and 39382.26 ppm) and Al (14573.92, 16685.85, and 16685.44 ppm) in the stream, beach, and rock magnetite samples, respectively (Tables 4, 5, 6 in Supplementary Information) may be attributable to high magnetite formation temperatures observed in this study (> 700 °C). Al exhibited a negative correlation with Fe ( $r = -0.82$ ) and Ti ( $-0.36$ ), whereas Fe exhibited a positive correlation with Ti (0.09). These correlations may be attributable to the absence of hercynite ( $\text{FeAl}_2\text{O}_4$ ) in the study area. Cr and Ni demonstrated a positive correlation with Fe ( $r = 0.28$  and  $0.22$ , respectively) and a negative correlation with Al ( $r = -0.25$  and  $-0.57$ , respectively). These correlations may be attributable to variations in magnetite present in the study area, including ulvöspinel ( $\text{Fe}_2\text{TiO}_4$ ), ilmenite ( $\text{FeTiO}_3$ ), chromite ( $\text{FeCr}_2\text{O}_4$ ), and trevorite ( $\text{NiFe}_2\text{O}_4$ ). Mg, Mn, and Zn demonstrated a negative correlation with Fe ( $r = -0.89$ ,  $-0.45$ , and  $-0.41$ , respectively) and a positive correlation with Al ( $r = 0.88$ ,  $0.28$ , and  $0.67$ , respectively; Table 10 in Supplementary Information). This correlation may be attributable to large variations in spinel series in the study area, including gahnite ( $\text{ZnAl}_2\text{O}_4$ ), spinel ( $\text{MgAl}_2\text{O}_4$ ), and galaxite ( $\text{MnAl}_2\text{O}_4$ ); however,

magnesioferrite ( $\text{MgFe}_2\text{O}_4$ ), jacobite ( $\text{MnFe}_2\text{O}_4$ ), and franklinite ( $\text{ZnFe}_2\text{O}_4$ ) were not noted in the study area.

Other elements including V, Co, Mo, Nb, Ga, Sn, and Ta exhibited a positive correlation with Fe but a negative correlation with Al (Table 10 in Supplementary Information). This correlation can be attributed to the enrichment of these elements in the magnetite series. Ca, Li, Sc, Cu, As, Rb, Sr, Y, Cd, Sb, Sc, Ba, REE, Pb, U, and Th demonstrated a negative correlation with Fe and a positive correlation with Al (Table 10 in Supplementary Information). This correlation can be attributed to the enrichment of these elements in the spinel series. REEs demonstrated a negative correlation with Fe and a positive correlation with Al. REEs were enriched in the spinel series.

## 5.2 Magnetite provenance

SEM revealed considerable similarity in the chemical composition of magnetite present in rocks surrounding the beach, stream, and rock samples. The chemical composition of magnetite in andesite rocks in the Keelung Mountain region (Fig. 1B; Table 3 in Supplementary Information) is similar to that found in Keelung Mountain Creek (Fig. 2G; Table 3 in Supplementary Information). This finding suggested that magnetite in this region originated from surrounding andesitic rocks. This speculation was confirmed by the chemical composition determined using LA-ICP-MS (Tables 4, 6 in Supplementary Information; Fig. 11). Similarly, the chemical composition of magnetite in chloritized andesite rocks in ChinKuashih Panshan Geological Park (Fig. 1C; Table 3 in Supplementary Information) is similar to that found in ChinKuashih Panshan Geological Park Creek (Figs. 2H, 3D; Table 3 in Supplementary Information) and Longdong Bay Creek. This finding suggests that chloritization andesite rocks are the source of magnetite in both ChinKuashih Panshan Geological Park Creek and Longdong Bay Creek; this was confirmed by the chemical composition determined using LA-ICP-MS (Tables 4, 6 in Supplementary Information; Fig. 12). Furthermore, we realized that the chemical composition of magnetite in andesite rocks in the White Sand Bay region (Fig. 2D; Table 3 in Supplementary Information) is similar to that in several adjacent beaches such as White Sand Bay, Laomei, and Xinzhuangzi as well as White Sand Bay Creek (Figs. 1H, 2D, F, 3F and Table 3 in Supplementary Information, respectively). This finding indicates that the andesite rock surrounding the region is the source of magnetite in these beaches and this creek; this was confirmed by the chemical composition determined using LA-ICP-MS (Tables 4, 5, 6 in Supplementary Information; Fig. 13). We found that the chemical composition of magnetite in Bianshan Fuan Palace (Guanyin Mountain) region (Fig. 2D in



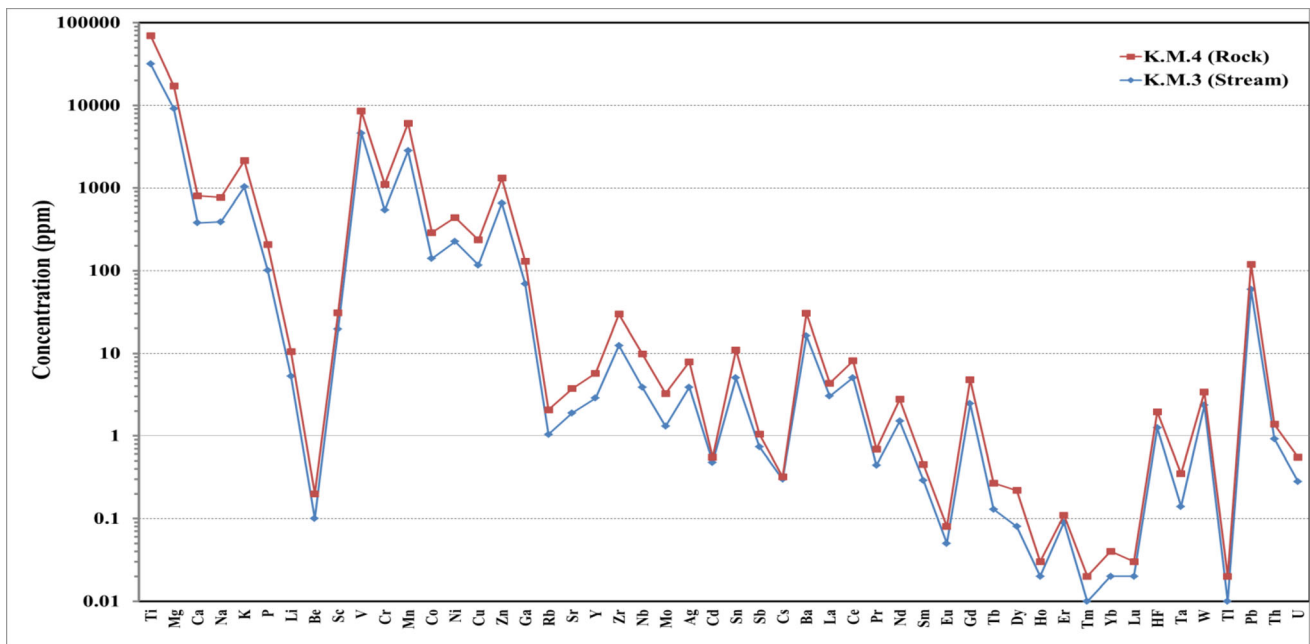


**Fig. 11** Compatibility of the chemical composition of magnetite present in the andesite rock in the Keelung Mountain area and the chemical composition of stream magnetite sediments present in the Keelung Mountain Creek

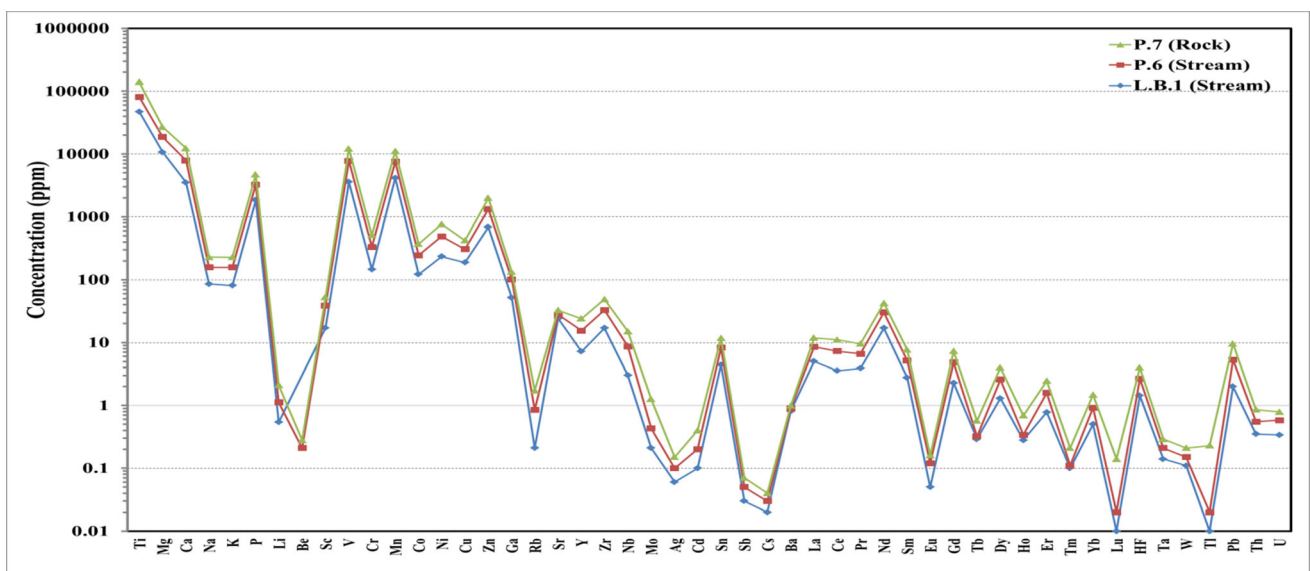


**Fig. 12** Compatibility of the chemical composition of magnetite present in the chloritization andesite rock in ChinKuashih Penshan Geological Park and the chemical composition of stream magnetite sediments in ChinKuashih Penshan Geological Park Creek and Londong Bay Creek

Supplementary Information) is similar to that of Shisan Hun Beach, Guanyin Beach, Linkou Creek, and Bianshan Fuan Palace (Guanyin Mountain) Creek (Figs. 2C, 2E, 3A, E, and Table in Supplementary Information, respectively). This finding indicated that basaltic andesite rocks are the source of magnetite in these beaches and streams; this was confirmed by the chemical composition determined using LA-ICP-MS (Tables 4, 5, 6 in Supplementary Information; Fig. 14). The chemical composition of magnetite in the Cai

Gongkeng region (Fig. 1E; Table 3 in Supplementary Information) is similar to that in the Fengyu Beach, Wanli Fishing Port Seaside Beach, Qingshan Waterfall, and Cai Gongkeng Creek (Figs. 2A, B, 3B, C and Table 3 in the Supplementary Information, respectively); this finding was confirmed by the chemical composition determined using LA-ICP-MS (Tables 4, 5, 6 in Supplementary Information; Fig. 15). However, we realized no similarity in the chemical composition of magnetite found in chloritized andesite

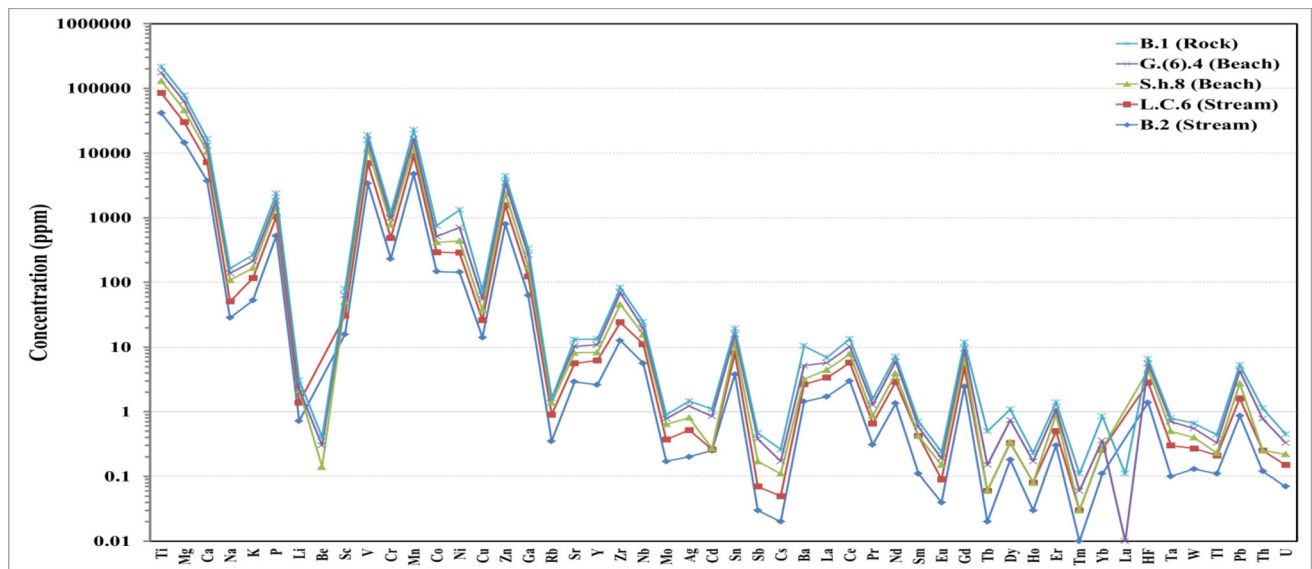


**Fig. 13** The compatibility of the chemical composition of magnetite present in the andesite rock in White Sand Bay with magnetite present in several adjacent beaches such as White Sand Bay, Laomei, and Xinzhuangzi beaches, and stream magnetite sediments in White Sand Bay Creek

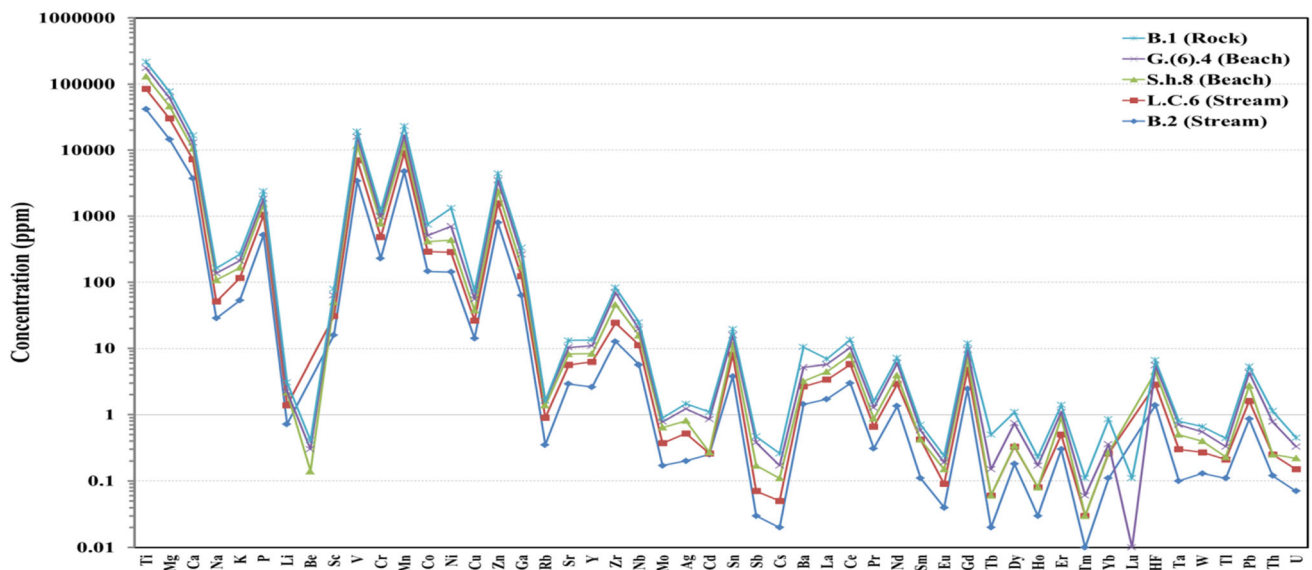


**Fig. 14** The compatibility of the chemical composition of magnetite present in the basaltic andesite rock in Bianshan Fuan Palace (Guanyin Mountain) region with Shisan Hun and Guanyin Beaches and Linkou and Bianshan Fuan Palace (Guanyin Mountain) creeks

and andesite rocks in the Wudan Mountain and Qingshan Waterfall regions (Fig. 1F, G and Table 3 in the Supplementary Information, respectively) with any of the magnetite found in beaches or creeks in these regions. In addition, in Longdong Bay, we could not obtain a rock slice with only one grain of magnetite for analysis. Because of the lack of magnetite, we determined the chemical composition of meta sandstone rocks found in the WF area in this region. Therefore, the meta sandstone rocks surrounding the Longdong Bay were not considered to be the source of magnetite in Longdong Bay Creek. The

magnetite chemical composition of Longdong Bay Creek (Fig. 3D; Table 3 in Supplementary Information) is similar to that found in the chloritization andesite rocks of ChinKuashih Panshan Geological Park (Fig. 1B; Table 3 in Supplementary Information); this finding was confirmed by the chemical composition determined using LA-ICP-MS (Tables 4, 6 in Supplementary Information; Fig. 15). The meta sandstone rocks in Longdong Bay and the chloritization andesite rocks in ChinKuashih Panshan Geological Park belong to the WF area.

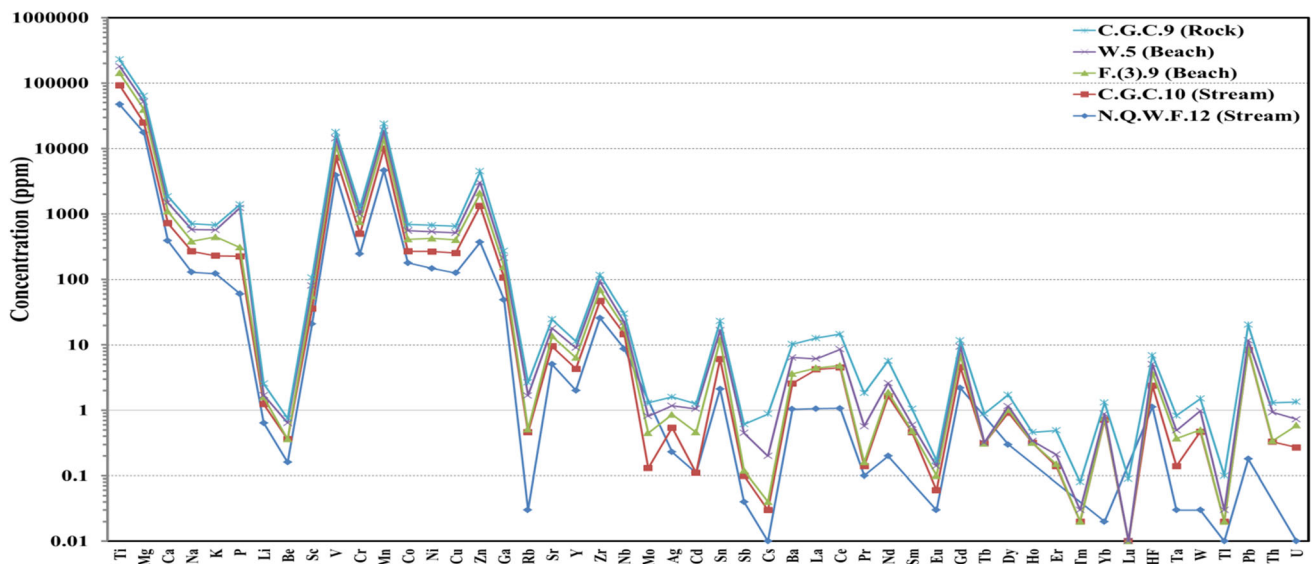


**Fig. 15** The compatibility of the chemical composition of magnetite present in the andesite rock in the Cai Gongkeng region with the Fengyu and Wanli Fishing Port Seaside beaches and Near Qingshan Waterfall and Cai Gongkeng Creeks

## 6 Conclusion

The results of this study revealed increased magnetite concentrations in the far north of Taiwan, especially in Wanli, Fengyu, Laomei, White Sand Bay Creek, White Sand Bay Beach, and Xinzhuangzi, and decreased magnetite concentrations toward the south and west of the study area. Generally, increased magnetite concentrations were observed around andesite rocks. Using the diagram developed by Dare et al. (2014), the studied samples were determined to be present within the magmatic field. In addition, we observed that the concentrations of Ti, Al, Mg, Sc, V, Cr, Mn, Co, Ni, Cu, Zn, Ga, Sn, Nb, Hf, and Ni/Cr in these samples were considerably similar to those in magnetite found in andesite rocks. This finding indicated that these studied magnetite samples may have originated from surrounding andesite rocks. Using the two diagrams developed by Dupuis and Beaudoin (2011), we plotted the studied samples within the Fe–Ti–V field. The chemical composition of magnetite found in the study samples is similar to that of Fe–Ti–V–P deposits hosted in mafic–ultramafic layered intrusions (Bushveld Complex, South Africa, and Sept Iles, Canada). All magnetite at the studied beach sand and some stream samples were titanomagnetite (ulvöspinel) because of the presence of a high Ti concentration. These titanomagnetites may be in the stage of transforming to many spinel minerals such as galaxite, gahnite, magnesiochromite, and chromite according to the high concentrations of Al, Ti, Mg, Cr, Ni, Mn, and Zn.

The different types of rocks surrounding these streams and beaches were determined to be the sources of magnetite grains found in the stream and beach samples.

Magnetite is believed to originate from surrounding magnetite-bearing rocks in north Taiwan. We determined the following sources of magnetite in different areas:

- (1) Andesite rocks surrounding the region as the source of magnetite in Keelung Mountain Creek; the chloritized andesite rock present in the ChinKuashih Panshan Geological Park region as the source of magnetite in both ChinKuashih Panshan Geological Park Creek and Longdong Bay Creek.
- (2) Andesite rocks surrounding the region as the source of magnetite in White Sand Bay Beach, Laomei Beach, Xinzhuangzi Beach, and White Sand Bay Creek; basaltic andesite in Bianshan Fuan Palace (Guanyin Mountain) region as the source of magnetite in the Shisan Hun Beach, Guanyin Beach, Linkou Creek, and Bianshan Fuan Palace (Guanyin Mountain) creek.
- (3) Basaltic andesite in the Cai Gongkeng region as the magnetite source in Fengyu Beach, Wanli Fishing Port Seaside Beach, Qingshan Waterfall, and Cai Gongkeng Creek.
- (4) We did not observe any similarity in the chemical composition of magnetite in chloritized andesite and andesite rocks found in the Wudan Mountain and Qingshan Waterfall regions (Fig. 1F and G in the Appendix, respectively) with that of magnetite found in beaches or creeks in these regions.
- (5) In the Longdong Bay region, we could not obtain a rock slice with only one grain of magnetite for analysis. Because of the lack of magnetite, we used the meta sandstone belonging to the WF unit in this region to determine the chemical composition.



Therefore, the meta sandstone rocks surrounding Longdong Bay are not considered to be the source of magnetite in Longdong Bay Creek. The chemical composition of magnetite in Longdong Bay Creek is similar to that in chloritization andesite rocks in ChinKuashih Panshan Geological Park. The meta sandstone in Longdong Bay and chloritization andesite rocks in ChinKuashih Panshan Geological Park belong to the WF unit (Table 2 in Supplementary Information; Figs. 1, 6).

In multielement variation diagrams, we concluded that Al, Cu, Ga, Hf, and Zn were highly enriched; most of the elements consistently exhibited the lowest concentrations, including Zr, Sc, Ta, Nb, Cu, Mo, Sn, Mn, Mg, Ti, Co, V, Ni, and Cr. The enrichment of Ca, Y, Pb, and W in our samples is the same as that reported by Dare et al. (2014) in andesitic magnetite found inside the magmatic magnetite field from intermediate magmas. The positive correlation between Fe and Ti and between Cr and Ni and the negative correlation between Fe and Mg and between Mn and Zn indicate the presence of various magnetite series in the study area, namely ulvöspinel ( $\text{Fe}_2\text{TiO}_4$ ), ilmenite ( $\text{FeTiO}_3$ ), chromite ( $\text{FeCr}_2\text{O}_4$ ), and trevorite ( $\text{NiFe}_2\text{O}_4$ ). These series might be attributed to the positive correlation of Fe with Ti, Cr, and Ni. The presence of gahnite ( $\text{ZnAl}_2\text{O}_4$ ), spinel ( $\text{MgAl}_2\text{O}_4$ ), and galaxite ( $\text{MnAl}_2\text{O}_4$ ) might be attributed to the positive correlation of Al with Mg, Mn, and Zn. The absence of hercynite ( $\text{FeAl}_2\text{O}_4$ ) might be attributed to the negative correlation of Fe with Al. Furthermore, the absence of magnesioferrite ( $\text{MgFe}_2\text{O}_4$ ), jacobsonite ( $\text{MnFe}_2\text{O}_4$ ), and franklinite ( $\text{ZnFe}_2\text{O}_4$ ) might be attributed to the negative correlation of Fe with Mg, Mn, and Zn. Other elements such as V, Co, Mo, Nb, Ga, Sn, and Ta exhibited a positive correlation with Fe. This finding may be attributed to the enrichment of these elements in magnetite series. The positive correlation of Ca, Li, Sc, Cu, As, Rb, Sr, Y, Cd, Sb, Sc, Ba, REE, Pb, U, and Th with Al may be attributed to the enrichment of these elements in the spinel series.

**Supplementary Information** The online version contains supplementary material available at <https://doi.org/10.1007/s11631-021-00521-y>.

**Acknowledgements** We thank GeoLasPro HD; Wuhan Shangpu Analytical Technology, Co., China, and Canada-Vancouver Lab (Mineral Laboratories, Bureau Veritas Commodities Canada, Ltd.) for their help in the LA-ICP-MS and ICP-MS analyses. We acknowledge constructive comments and suggestions from the Wallace Academic Editing to improve the English language. We give special thanks to anonymous journal reviewers for their constructive comments and suggestions.

**Author contributions** EM: conceptualization (lead), data curation (lead), formal analysis (lead), investigation (lead), methodology

(lead), writing—original draft (lead), writing—review and editing (lead); B-Sh: conceptualization (supporting), investigation (supporting), methodology (supporting), project administration (lead), writing—review and editing (supporting).

**Funding** This article is a personal work and does not belong to a project, so there is no funding for it.

**Data availability** All data generated and analyzed during this study are included in this published article and its Supplementary Information files.

**Code availability** Not applicable. Consent for publication Yes.

## Declarations

**Conflict of interest** On behalf of all authors, the corresponding author states that there is no conflict of interest.

**Ethical approval** Not applicable.

**Informed consent** Yes.

## References

- Abdullah MI, Atherton MP (1964) The thermometric significance of magnetite in low-grade metamorphic rocks. *Am J Sci* 262:904–917
- Alva-Vadivia LM, Rivas ML, Goguitchaichvili A, Urrutia-Fucugauchi J, Gonzalez JA, Morales J, Gómez S, Henríquez F, Nyström JO, Naslund RH (2003) Rock-magnetic and oxide microscopic studies of the El Laco ore deposits, Chilean Andes, and implications for magnetic anomaly modeling. *Int Geol Rev* 45:533–547
- Balan E, De Villiers JP, Eeckhout SG, Glatzel P, Toplis MJ, Fritsch E (2006) The oxidation state of vanadium in titanomagnetite from layered basic intrusions. *Am Mineral* 91:953–956
- Barnes SJ, Roeder PL (2001) The range of spinel composition in terrestrial mafic and ultramafic rocks. *J Petrol* 42:2279–2302
- Broughm SG, Hanchar JM, Tornos F, Westhues A, Attersley S (2017) Mineral chemistry of magnetite from magnetite–apatite mineralization and their host rocks: examples from Kiruna, Sweden, and El Laco, Chile. *Miner Depos* 52(8):1223–1244
- Buddington AF, Lindsley DH (1964) Iron–titanium oxide minerals and synthetic equivalents. *J Petrol* 5:310–357
- Canil D, Grondahl C, Lacourse T, Pisiak LK (2016) Trace elements in magnetite from porphyry Cu–Mo–Au deposits in British Columbia, Canada. *Ore Geol Rev* 72:1116–1128
- Chen CH, Wu YT (1971) Volcanic geology of the Tatun Geothermal Area, northern Taiwan. *Proc Geol Soc China* 14:5–28
- Chiaradia M, Müntener O, Beate B (2011) Enriched basaltic andesites from mid-crustal fractional crystallization, recharge, and assimilation (Pilavo Volcano, Western Cordillera of Ecuador). *J Petrol* 52:1107–1141
- Dare SA, Barnes S-J, Beaudoin G (2012a) Variation in the trace element content of magnetite crystallized from a fractionating sulfide liquid, Sudbury, Canada: implications for provenance discrimination. *Geochim Cosmochim Acta* 88:27–50
- Dare SA, Barnes S-J, Beaudoin G (2012b) Did the massive magnetite Blava Flows of El Laco (Chile) form by magmatic or hydrothermal processes? New constraints from magnetite composition by LA-ICP-MS. *Miner Depos* 50:607–617

- Dare SA, Barnes S-J, Beaudoin G, Méric J, Boutroy E, Potvin-Doucet C (2014) Trace elements in magnetite as petrogenetic indicators. *Miner Depos* 49:785–796
- Deditius AP, Reich M, Simon AC, Suvorova A, Knipping J, Roberts MP, Rubanov S, Dodd A, Saunders M (2018) Nanogeochemistry of hydrothermal magnetite. *Contrib Mineral Petrol* 173:46
- Duparc Q, Dare SA, Cousineau PA, Goutier J (2016) Magnetite chemistry as a provenance indicator in Archean Metamorphosed Sedimentary Rocks. *J Sediment Res* 86(5):542–563
- Dupuis C, Beaudoin G (2011) Discriminant diagrams for iron oxide trace element fingerprinting of mineral deposit types. *Miner Depos* 46:319–335
- Edfelt A, Armstrong RN, Smith M, Martinsson O (2005) Alteration paragenesis and mineral chemistry of the Tjarrojakka Apatite-iron and Cu–Au occurrences, Kiruna area, northern Sweden. *Miner Depos* 40:409–434
- Edmonds M, Brett A, Herd R, Humphreys M, Woods A (2015) Magnetite-bubble aggregates at mixing interfaces in andesite magma bodies. *Geol Soc Lond Spec Publ* 410(1):95–121
- Ghiorso MS, Sack O (1991) Fe–Ti oxide geothermometry: thermodynamic formulation and the estimation of intensive variables in silicic magmas. *Contrib Mineral Petrol* 108:485–510
- Ghose J, Hallam GC, Read DA (1977) A magnetic study of FeGa<sub>2</sub>O<sub>4</sub>. *J Phys C* 10:1051
- Gregory MJ (2006) Copper mobility in the Eastern Creek Volcanics, Mount Isa, Australia: evidence from laser ablation ICP-MS of iron–titanium oxides. *Miner Depos* 41:691–711
- Grigsby JD (1990) Detrital magnetite as a provenance indicator. *J Sediment Petrol* 60:940–951
- Groves DI, Bierlein FP, Meinert LD, Hitzman MW (2010) Iron oxide copper–gold (IOCG) through Earth’s history: implications for origin, lithospheric setting, and distinction from other epigenic iron oxide deposits. *Econ Geol* 105:641–654
- Henríquez F, Martin RF (1978) Crystal growth textures in magnetite flows and feeder dykes, El Laco, Chile. *Can Mineral* 16:581–589
- Hitzman MW (2000) Iron oxide–Cu–Au deposits: what, where, when, and why. In: Porter TM (ed) *Hydrothermal iron oxide copper–gold and related deposits a global perspective*. PGC Publications, pp 9–26
- Hu X, Chen H, Beaudoin G, Zhang Y (2020) Textural and compositional evolution of iron oxides at Mina Justa (Peru): implications for mushketovite and formation of IOCG deposits. *Am Mineral* 105:397–408
- Huang XW, Zhou MF, Qi L, Gao JF, Wang YW (2013) Re–Os isotopic ages of pyrite and chemical composition of magnetite from the Cihai magmatic–hydrothermal Fe deposit, NW China. *Miner Depos* 48:925–946
- Knipping JL, Bilinker LD, Simon AC, Reich M, Barra F, Deditius AP, Walle M, Heinrich CA, Holtz F, Munizaga R (2015) Trace elements in magnetite from massive iron oxide-apatite deposits indicate a combined formation by igneous and magmatic–hydrothermal processes. *Geochim Cosmochim Acta* 171:15–38
- Li BL, Xie YH (1984) Origin, classification and metallogenic model of Ningwu porphyry-type iron deposits. *Sci China* 1:80–86 (in Chinese with English abstract)
- Lin Ch-W, Chen W-Sh (2016) Geologic map of Taiwan. Geological Society of Taiwan
- Lindsley DH (1976a) Experimental studies of oxide minerals. *Rev Mineral* 3:L61–L88
- Lindsley DH (1976b) The crystal chemistry and structure of oxide minerals as exemplified by the Fe–Ti oxides. *Rev Mineral* 3:L1–L60
- Lindsley DH (1991) Experimental studies of oxide minerals. *Rev Mineral* 25:69–100
- Louis S, Teng C, Lee T, Ch-Hs P, Chen W-F, Chu C-J (2001) Origin and geological evolution of the Taipei Basin, northern Taiwan. *West Pac Earth Sci* 1(2):115–142
- Luepke G (1980) Opaque minerals as aids in distinguishing between source and sorting effects on beach-sand mineralogy in southwestern Oregon. *J Sediment Petrol* 50:489–496
- Maier WD, Barnes S-J (1996) Unusually high concentrations of magnetite at Caraiba and other Cu-sulfide deposits in the Curaca Valley, Bahia, Brazil. *Can Mineral* 34:717–731
- Martinsson O, Billström K, Broman C, Weihed P, Wanhainen C (2016) Metallogeny of the Northern Norrbotten Ore Province, northern Fennoscandian shield with emphasis on IOCG and apatite-iron ore deposits. *Ore Geol Rev*. <https://doi.org/10.1016/j.oregeorev.2016.02.011>
- McIntire WL (1963) Trace element partition coefficients—a review of theory and applications to geology. *Geochim Cosmochim Acta* 27:1209–1264
- Mollo S, Putirka K, Iezzi G, Scarlato P (2013) The control of cooling rate on titanomagnetite composition: implications for a geospeedometry model applicable to alkaline rocks from Mt Etna Volcano. *Contrib Mineral Petrol* 165:457–475
- Morton AC (1991) Geochemical studies of detrital heavy minerals and their application to provenance research. In: Morton AC, Todds SP, Haughton PDW (eds) *Developments in sedimentary provenance studies*. Special Publication 57. Geological Society of London, p 31–45
- Morton AC, Hallsworth CR (1994) Identifying provenance-specific features of detrital heavy mineral assemblages in sandstones. *Sediment Geol* 90:241–256
- Nadoll P, Koenig AE (2011) LA-ICP-MS of magnetite: methods and reference materials. *J Anal at Spectrom* 26:1872–1877
- Nadoll P, Mauk JL, Hayes TS, Koenig AE, Box SE (2012) Geochemistry of magnetite from hydrothermal ore deposits and host rocks of the Mesoproterozoic Belt Supergroup, United States. *Econ Geol* 107:1275–1292
- Nadoll P, Angerer T, Mauk JL, French D, Walshe J (2014) The chemistry of hydrothermal magnetite: a review. *Ore Geol Rev* 61:1–32
- Nadoll P, Mauk JL, Leveille RA, Koenig AE (2015) Geochemistry of magnetite from porphyry Cu and Skarn deposits in the southwestern United States. *Miner Depos* 50:493–515
- Namur O, Charlier B, Toplis M, Higgins MD, Liégeois JP, Van der Auwera J (2010) Crystallization sequence and magma chamber processes in the ferrobaltic Sept Iles layered intrusion, Canada. *J Petrol* 51:1203–1236
- Naslund HR, Henríquez FJ, Nyström JO, Vivallo W, Dobbs F (2002) Magmatic iron ores and associated mineralization: examples from the Chilean high Andes and Coastal Cordillera. In: Porter TM (ed) *Hydrothermal iron oxide copper–gold and related deposits: a global perspective*, vol 2. PGC Publishing, Adelaide, pp 207–226
- Nielsen RL, Forsythe LM, Gallahan WE, Fisk MR (1994) Major and trace element magnetite–melt equilibria. *Chem Geol* 117:167–191
- Nyström JO, Henríquez F (1994) Magmatic features of iron ores of the Kiruna type in Chile and Sweden; ore textures and magnetite geochemistry. *Econ Geol* 89:820–839
- Nyström JO, Billström K, Henríquez F, Fallick AE, Naslund HR (2008) Oxygen isotope composition of magnetite in iron ores of the Kiruna type in Chile and Sweden. *GFF* 130:177–188
- O’Neill HSC, Navrotsky A (1984) Cation distributions and thermodynamic properties of binary spinel solid solutions. *Am Mineral* 69:733–753
- Park JW, Campbell IH, Ickert RB, Allen CM (2013) Chalcophile element geochemistry of the Boggy Plain zoned pluton,

- southeastern Australia: an S-saturated barren compositionally diverse magmatic system. *Contrib Mineral Petrol* 165:217–236
- Paton C, Hellstrom J, Paul B, Woodhead J, Hergt J (2011) Iolite: freeware for the visualization and processing of mass spectrometric data. *J Anal at Spectrom* 26:2508–2518
- Pettijohn FJ, Potter PE, Siever R (1987) *Sand and sandstone*, 2nd edn. Springer, New York, p 553
- Pisiak LK, Canil D, Lacourse T, Plouffe A, Ferbey T (2017) Magnetite as an indicator mineral in the exploration of porphyry deposits: a case study in till near the Mount Polley Cu–Au Deposit, British Columbia, Canada. *Econ Geol* 112(4):919–940
- Rapp JF, Klemme S, Butler IB, Harley SL (2010) Extremely high solubility of rutile in chloride and fluoride-bearing metamorphic fluids: an experimental investigation. *Geology* 38:323–326
- Razjigaeva NG, Naumova V (1992) Trace element composition of detrital magnetite from coastal sediments of Northwestern Japan Sea for provenance study. *J Sediment Petrol* 62:802–809
- Reguir EP, Chakhmouradian AR, Halden NM, Yang P (2008) Early magmatic and reaction-induced trends in magnetite from the carbonatites of Kerimasi, Tanzania. *Can Mineral* 46:879–900
- Righter K, Leeman WP, Hervig RL (2006) Partitioning of Ni, Co, and V between spinel-structured oxides and silicate melts: importance of spinel composition. *Chem Geol* 227:1–25
- Rollinson HR (1993) *Using geochemical data: evaluation, presentation, interpretation*. Longman Scientific and Technical, London
- Rumble D (1976) Oxide minerals in metamorphic rocks. *Rev Mineral* 3:R1–R20
- Rusk BG, Oliver N, Brown A, Lilly R, Jungmann D (2009) Barren magnetite breccias in the Cloncurry region, Australia; comparisons to IOCG deposits. In: *Society for Geology Applied to Mineral Deposits, 10th biennial SGA meeting, proceedings*, Townsville, Australia, pp 656–658
- Ryabchikov ID, Kogarko LN (2006) Magnetite compositions and oxygen fugacities of the Khibina Magmatic System. *Lithos* 91:35–45
- Salazar E, Barra F, Reich M, Simon A, Leisen M, Palma G, Romero R, Rojo M (2019) Trace element geochemistry of magnetite from the Cerro Negro Norte Iron Oxide–Apatite Deposit, northern Chile. *Miner Depos* 55:409–428
- Shane P (1998) Correlation of rhyolitic pyroclastic eruptive units from the Taupo Volcanic Zone by Fe–Ti oxide compositional data. *Bull Volcanol* 60:224–238
- Song SR, Tsao ST, Lo HJ (2000) Characteristics of the Tatum Volcanic Eruptions, northern Taiwan: implications for a cauldron formation and volcanic evolution. *J Geol Soc China* 43:361–378
- Sun W, Yuan F, Jowitt SM, Zhou T, Liu G, Li X, Wang F, Trolls VR (2019) In situ LA–ICP–MS trace element analyses of magnetite: genetic implications for the Zhonggu Orefield, Ningwu Volcanic Basin, Anhui Province, China. *Miner Depos* 54:1243–1264
- Taylor SR, McLennan SM (1985) *The continental crust: its composition and evolution*. Blackwell, Oxford, p 312
- Teng LS, Chen CH, Wang WS, Liu TK, Juang WS, Chen JC (1992) Plate kinematic model for Late Cenozoic Arc magmatism in northern Taiwan. *J Geol Soc China* 35:1–18
- Teng LS, Lee CT, Peng CH, Chen WF, Chu CJ (2001) Origin and geological evaluation of the Taipei Basin, Northern Taiwan. *West Pac Earth Sci* 1(2):115–142
- Toplis M, Carroll M (1995) An experimental study of the influence of oxygen fugacity on Fe–Ti oxide stability, phase relations, and mineral–melt equilibria in ferro-basaltic systems. *J Petrol* 36:1137–1170
- Toplis M, Corgne A (2002) An experimental study of element partitioning between magnetite, clinopyroxene, and iron-bearing silicate liquids with particular emphasis on vanadium. *Contrib Mineral Petrol* 144:22–37
- Tornos F, Velasco F, Hanchar JM (2016) Iron oxide melts, magmatic magnetite and superheated magmatic–hydrothermal systems: the El Laco Deposit, Chile. *Geology* 44(6):427–430
- Waychunas GA (1991) Crystal chemistry of oxides and oxyhydroxides. *Rev Mineral* 25:11–61
- Wood BJ, Nell J, Woodland AB (1991) Macroscopic and microscopic thermodynamic properties of oxides. *Rev Mineral* 25:265–302
- Yang S, Wang Z, Gui Y, Li C, Cai J (2009) Heavy mineral compositions of the Changjiang (Yangtze River) sediments and their provenance tracing implication. *J Asian Earth Sci* 35:56–65
- Zhang Y, Hollings P, Shao Y, Li D, Chen H, Li H (2020) Magnetite texture and trace-element geochemistry fingerprint of pulsed mineralization in the Xinqiao Cu–Fe–Au Deposit, Eastern China. *Am Mineral* 105(11):1712–1723